Fuel 236 (2019) 404–427

Contents lists available at ScienceDirect

Fuel

journal homepage: www.elsevier.com/locate/fuel

Review article

A review of the current progress of CO_2 injection EOR and carbon storage in shale oil reservoirs

Bao Jia*, Jyun-Syung Tsau, Reza Barati

University of Kansas, United States

ARTICLE INFO

Keywords:
Shale oil
Gas injection
Fracture
Numerical modeling
PVT
Shale petrophysics

ABSTRACT

CO_2 injection is a promising method to rejuvenate the shale oil reservoirs after the primary production. In this work, we comprehensively reviewed the CO_2 injection enhanced oil recovery (EOR) and carbon storage related literature in shales over the past decade. The aspects reviewed include description of major shale reservoirs producing oil and the necessity to perform EOR, selection of injection scheme, models applied to simulate gas injection, oil recovery mechanisms for different types of gas, molecular diffusion and its laboratory measurement, nanopore effect, adsorption effect on carbon storage and transport, laboratory work of gas injection in shale cores, pilot tests, and economic evaluation. Advanced models in recent years applied to simulate these processes were introduced in details, such as the traditional dual continuum model, the embedded discrete fracture model (EDFM). Heterogeneity effect and upscaling algorithm on the shale oil recovery performance were discussed. Molecular diffusion, as an important flow and oil recovery mechanism, was described regarding its definition, empirical correlation and laboratory measurement with consideration of the porous media effect which is crucial for accurate modeling result. Recovery mechanisms by carbon dioxide, methane and nitrogen were compared at the molecule and pore levels. Pros and cons of different types of gas were evaluated as well. Pore confinement caused by the extremely tiny pores in the organic matter, along with the capillary and adsorption effects were discussed, and approaches to take them into account of the model were addressed. Core-scale gas injection experiments on shales from various institutions were described, and the results were compared. Outcomes of recent pilot tests in the Eagle Ford, and the Bakken formations were summarized, and finally, economic considerations were provided for the feasibility of gas injection in shale oil reservoirs.

1. Introduction

The fraction of import of net crude oil and petroleum-related production in the U.S. decreases during the recent years, which is contributed mostly to the development of tight oil reservoirs [1]. With projections to 2040 in the reference case, tight oil will be dominating over the non-tight oil. Table 1 shows several major arising plays in the U.S. that are extensively tight oil. The Bakken play is comprised of three parts: lower, middle and upper Bakken [2]. The upper and lower Bakken are classified as the world-class source rock, and the middle Bakken is the primary production zone. The Bakken play is relatively thin lying in the central and deep part of the Williston Basin that it includes both conventional and unconventional parts. It covers across states of Montana, North Dakota in the northern central America and provinces of Saskatchewan and Manitoba in south-central Canada. The originally oil in place (OOIP) is estimated between 300 Bbbl [3] and 900 Bbbl [4] and the technical recoverable reserve is estimated to be between 4.5 Bbbl and 20 Bbbl [5]. Kerogen type is mainly Type II [6]. The kerogen type is defined based on the ratio between the hydrogen index and oxygen index. The higher the ratio, the higher quality the kerogen is, meaning that it is more oil prone. Type I is oil-prone, type II is oil and gas prone, type III is gas prone, and type IV is neither oil or gas prone [6]. In 1996, the first Albin wells were successfully completed in the Middle Bakken. In 2000, the Elm Coulee was discovered, and the

Abbreviations: AD-GPRS, automated differentiation based general purpose research simulator; CCS, carbon capture and storage; CT, computed tomography; DFIT, diagnostic fracture injection test; DFT, density function theory; DK, double-porosity; DP, double-permeability; EDFM, embedded discrete fracture model; EERC, Energy & Environmental Research Center; EOR, enhance oil recovery; GOR, gas oil ratio; LGR, local grid refinement; MINC, multiple interacting continua model; MMP, minimum miscible pressure; MRI, magnetic resonance imaging; NMR, Nuclear Magnetic Resonance; NPV, net present value; OOIP, originally oil in place; PNL, pulse-neutron log; PSD, pore size distribution; SRV, stimulated reservoir volume; TOC, total organic carbon; TRR, technically recoverable resources; USI, ultrasonic imager; VLE, vapor-liquid equilibrium; WAG, water alternating gas

* Corresponding author.
E-mail addresses: baojia@ku.edu (B. Jia), rezab@ku.edu.com (R. Barati).

https://doi.org/10.1016/j.fuel.2018.08.103
Received 9 May 2018; Received in revised form 29 July 2018; Accepted 24 August 2018
Available online 13 September 2018

Nomenclatures

C_0	initial investment
C_t	period cash inflow
D	diffusion coefficient
D_{eff}	effective diffusion coefficient
F	formation resistivity factor
FCO_2STR	amount of CO_2 stored subsurface
FICIT	purchasing and injection amount of CO_2
f^L	fugacity in the liquid phase
FOPT	produced amount of oil
f^V	fugacity in the vapor phase
FWPT	amount of produced water
J	molar flux
k	Lattice Boltzmann constant
k_a	apparent permeability
k_{50}	median in the permeability distribution spectrum
$k_{84.1}$	median added with one standard deviation
K_a	partition coefficient
l	distance
m	cementation factor
M	molecular weight
n_c	number of components
P_c	critical pressure
P_c	capillary pressure
P_{cp}	critical pressure with the pore confinement
P^L	liquid pressure
P^V	vapor pressure
R	period discount rate
r_p	pore size
S	saturation
T	temperature
t	time step
T_c	critical temperature
T_c	cumulative time
T_{cp}	critical temperature with the pore confinement
V_A	absolute adsorption
V_{bi}	partial molar volume at the boiling pressure
V_c	critical volume
V_{dp}	Dykstra–Parsons variation coefficient
V_G	Gibbs
X	fraction
x	faction in the liquid phase
y	fraction in the gas phase
z	fraction globally
Z_c	compressibility factor at critical state
ΔP_c	critical pressure shift
ΔT_c	critical temperature shift
ε	characteristic energy
ρ	density
ρ_a	density of the adsorption phase
ρ_g	density of the free gas
ρ^L	liquid density
ρ^V	vapor destiny
σ	Leonard-Jones potential parameter
σ_F	interfacial tension
τ	tortuosity
ϕ	porosity
ϕ_{void}	porosity consisting only of the void volume
ϕ_a	apparent porosity
ϕ_{app}	porosity in the adsorptive gas flowing equation
χ^i	parachor coefficient
Ω	collision integral
μ	viscosity

Table 1
Information of major shale oil plays in the US [5,11].

Play	Bakken	Eagle Ford	Niobrara	Utica	Wolfcamp
Area, mi^2	200,000	1000	14,000	170,000	98,000
Depth, ft	8500–10,000	4000–12,000	6000–8,000	2000–14,000	5500–11,000
Porosity, %	8–12	4–10	3	6–12	2–10
Pressure Gradient, psi/ft	0.50–0.60	0.50–0.75	0.42–0.60	0.6	0.55–0.70
Total organic carbon (TOC), %	9+	4–8	7–12	0.3–2.5	2–6
Thermal Maturity, R_0, %	0.6–1.0	0.7–1.8	0.5–1.4+ (Uneven cooking)	0.6	0.8
Thickness, ft	8–14	300–475	150–300	70–750	1500–2600
Cond Ratio, B/MMcf IP rate, MMcfd	200–1800	250–1500	400–500	4,5–17 MMcfd 200–1500 Bcpd	1050
EUR/Well, MBbl	700	600	250–450	3.6–5.4 Bcf	650–750
Avg Lateral, ft	8700–10,000	6000–7000	4050–5100	500–900	4550–6700
Well Spacing, Acres	160	40–80	160 (D/S 40)	160	80
TRR, Bbbl	4.5 (20)	7–10	1.5	3.0 (5.5)	30 (Ind. est.)
Well Cost, $MM	8.5–9.0+	6.0–9.0	3.5–5.5	6.0–8.0	7.0–8.0
First Production	2008 (Middle Bakken)	2006	2006	2011	2011

first horizontal well was drilled in the Middle Bakken. In 2006, the Parshall Field was discovered [7]. The first successful liquid production from the Bakken occurred in 2008. Until the end of 2014, producing wells in the Bakken tight oil has reached 7630 [5].

The Eagle Ford play lies in south Texas that it covers more than 20 counties across Mexico. The OOIP in the Eagle Ford is between the P90 5.3 Bbbl and P10 28.7 Bbbl [8]. Oil production from the Eagle Ford play, along with Austin Chalk contribute primarily in the region of onshore Gulf coast. Kerogen type is mainly Type II, the lithology in the Eagle Ford consists of about 15% silica, 70% carbonate, and 15% clay. The formation rock is relatively brittle for fracturing purpose. The Eagle Ford has significant storage of dry gas, wet gas, and oil resources that it has been one of most active plays in the US, till the end of 2014, producing wells have reached 5650 [5].

The Niobrara (and Codel) shale lies in the Wattenberg Field located in the northeast of Denver, Colorado, where both conventional and unconventional reservoirs exist. Niobrara B and C chalk and the Codel sandstone have been oil production zones for decades [9]. Drilling and multi-stage fracturing began in 2006–2007. Niobrara shale is located at about 7000 ft depth with the thickness ranging from 150 ft to 300 ft. The complex geological condition of the Niobrara shale makes it challenging to develop sweet spots and perform hydraulic fracturing. Until the middle of 2013, the number of well completion reached 874 [5].

The Utica shale is located in the northern part of US across several states. It has producing windows of dry gas, wet gas, and oil. It has a wide range of depth varying from 2000 ft to 14000 ft and a wide range of thickness varying from 70 ft to 750 ft. The technically recoverable resources (TRR) is estimated to be 3.0 [5].

The Wolfcamp shale in the Midland basin which is a major oil resource of the Permian basin with an OOIP of over 20 Bbbl that the F95 and F5 are 11 Bbbl and 31 Bbbl, respectively. Kerogen type varies significantly in the Wolfcamp shale: unit A and B are Type II and Type II/Type III mixing, unit C is mainly Type III and unit D is mainly Type II [10]. Until the end of 2014 and early 2015, the producing wells in the Wolfcamp shale reached 6101 and the rig count reached 215 [5].

Shale oil in place in China is estimated to be 643 Bbbl, and the technically recoverable amount is 32.2 Bbbl in three main basins of Junggar, Tarim, and Songliao [12]. Oil and wet-gas thermal maturity windows are available in the Junggar basin, the thickness and average TOC of which are about 984 ft and 4%, respectively. The fact that the depositional environment is lacustrine in the Junggar basin causes associated issues of fracability in this area. Evaluation of oil production potential in the adjacent Santanghu Basin has been performed by Shell, Hess, and China National Petroleum Corporation (CNPC) but no drilling activity has been seen until 2013 [12]. In the Tarim basin, horizontal wells have been well developed for conventionals, but not yet for unconventional shales until 2013, because of the remoteness of the interior region and the exploration difficulty. The Cambrian and Ordovician shales are rich in carbonate with only 1% to 2% TOC. In contrast, the Ordovician shale and Triassic mudstone have better oil storage potential [12]. In the Songliao basin, both oil and wet gas thermal maturity windows are available in the shale part which has high-density natural fracture network. Oil production potential evaluation has been performed at the Daqing field and horizontal drilling activity has been seen in the Jinlin field [12].

In Canada, the technically recoverable oil amount is 9 Bbbl [5]. A part of the Bakken play is located in Canada. Besides, the Duvernay shale in Canada has dry gas, wet gas, and oil thermal maturity windows. The Duvernay shale exhibits good fracability containing 15%–30% clays, making it an ideal target for hydraulic fracturing [5]. In the northern South America, the shale oil TRR is 20.2 Bbbl, among which Colombia and western Venezuela account for 6.8 Bbbl and 13.4 Bbbl, respectively. Colombia's La Luna shale has dry gas, wet gas, and oil thermal maturity windows, with TOC percentage of 2% to 5%. South America also has prospective shale oil storage potential. Argentina has shale oil TRR of 27 Bbbl where many companies have been drilling horizontal wells that optimistic results have been observed [5]. Brazil has shale oil TRR and in place of 5.4 Bbbl and 134 Bbbl, respectively. No drilling activity has been observed in shale formations until late 2014 in Brazil [5]. Mexico's shale oil TRR is estimated to be 6.3 Bbbl, most of which is concentrated in the region of Gulf of Mexico. Difficulties in producing shale oil in Mexico are contributed to several factors, including investment constraints, reservoir service capabilities, and safety issues. Europe also has optimistic shale oil storage. The shale oil TRR in Portland is 1.8 Bbbl. The shale oil in place in the United Kingdom is 54 Bbbl. Australia has shale oil risked TRR and in place of 17.5 Bbbl and 403 Bbbl, respectively. Russia has shale oil risked TRR and in place of 74.6 Bbbl and 1243 Bbbl, respectively. For more information of shale oil around the world, the reader can consult references [5] and [13].

Despite of the huge oil reserves in the unconventional reservoirs, all of them are facing an inevitable problem: short production life usually less than 10 years and a low recovery factor between 3% and 10%. Fig. 1 shows the oil wells' production history in North Dakota from 2007 to 2014. It could be observed that the oil production decreases rapidly from around 400 bbl/day to below 50 bbl/day after two years. To increase the oil recovery factor and reservoir energy, gas injection has been expected to be a promising method. From another perspective, gas injection EOR has the win-win effect of carbon capture and storage (CCS) if CO_2 is applied as the injection gas [14].

2. Different models of gas injection processes in shale reservoirs

Table 2 shows the representative modeling work of gas injection in unconventional reservoirs. It is observed that the modeling approach has evolved a lot over the past five years. It has been believed that compositional and dual-continuum approach results in more accurate simulation result for fractured shale reservoirs. Recent studies show advancements of more properly simulating fractures.

Properly dealing with the interaction between matrix and fracture is very important and sometimes very challenging [33,34]. Fractures in the tight and shale reservoirs can be classified as hydraulic fractures and natural fractures. Hydraulic fractures are generally in macro size, and natural fractures are generally in micro size [35,36]. Hydraulic fractures along with their stimulated complex fracture network increase the surface area between the wellbore and reservoir rocks; they greatly increase the drained reservoir volume and increase the economical production rate. To more efficiently design hydraulic fracture process, a Diagnostic Fracture Injection Test (DFIT) [37,38] is usually performed first to obtain important reservoir properties like fracture closure pressure, reservoir permeability, and reservoir pressure. It is important to create more efficient and conductive hydraulic fractures during the pumping period. Regions with the lithology that is more brittle and lower minimum horizontal stress are considered to have preferable fracking mechanical properties [39]. The microseismic data can be collected to measure the effectiveness of hydraulic fracture and the subsequent development of the fracture network [40–42]. Properties of the natural fracture network, including its location, orientation and important parameters for hydraulic fracture initiation. The existence of the natural fracture network is also of significance for the process of hydrocarbon extraction from the matrix to the hydraulic fracture and finally the wellbore [43]. As pointed out by Theloy et al. [44], the existence of natural fracture in the Bakken plays a significant role in oil production. Mullen et al. [43] demonstrated through simulation that the if the horizontal well is geosteered to optimize the spacing of swellable packers and fracture stage in the most natural fractured intervals of the Bakken formation, the oil recovery factor could be improved by 20%. Wan and Liu [45] studied the effects of fracture density and fracture conductivity on CO_2 huff-n-puff processes. They found that as long as the fracture conductivity is larger than the critical value of 4 mD-ft, the fracture density is more important than the fracture conductivity on improving oil recovery performance. Therefore, it is essential and challenging to appropriately model the complex fracture network due to its importance for unconventionals. Generally speaking, modeling complex fracture network falls into two categories: dual continuum approach and explicit fracture or discrete fracture model (DFM) approach. The dual continuum approach refers to the double-porosity (DP) and double-permeability (DK) models that initially

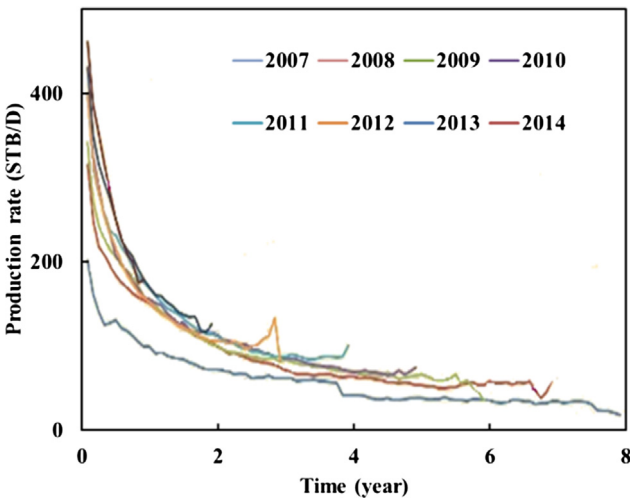

Fig. 1. Production decline profiles in the Bakken (Modified from Paterson [15]).

Table 2
Representative work of CO_2 huff-n-puff to recover shale oil (modified based on [16]).

Authors	Porosity	Permeability	Natural fracture	Hydraulic fracture	Model	Simulator
Chen [17]	6%	1E − 4 mD	NA	83.3 mD-ft	Single porosity	IMEX
Wan [18]	6%	1E − 5 mD	NA	83.3 mD-ft	Single porosity	IMEX
Kurtoglu [19]	5.6% (matrix), 0.22% (fracture, effective) - scenario in the Middle Bakken, homogeneous, and dual porosity	3E − 4 mD - scenario in the Middle Bakken, homogeneous, and dual porosity	SRV 0.0313 mD, USRV 0.00216 mD (effective) - scenario in the Middle Bakken, homogeneous, and dual porosity	Width 0.5 ft	Dual porosity and single porosity	in-house, name NA
Pu [20]	6.88%	SRV 0.1 mD USRV 0.05 mD (model #1)	NA	23 mD-ft, 16 mD × 1.44 ft -Model#1	Single porosity	IMEX
Fai-Yengo et al. [21]	10%	0.05 mD	NA	intrinsic permeability: 100,000 mD	Single porosity	NA
Chen et al. [22]	8% (matrix), 43% (fracture)	0.01 mD	NA	50 mD-ft, 10,000 mD × 0.005 ft	Single porosity	UT-COMP
Sanchez et al. [23]	8% (matrix), 43% (fracture)	0.01 mD	Five 2-ft width fracture, permeability 1 mD (base case)	50 mD-ft, 10,000 mD × 0.005 ft, psedudolized as 25 mD × 2 ft	Single porosity	GEM
Yu et al. [24]	5.60%	5E − 3 mD (base case)	NA	10 mD-ft (base case)	Single porosity	GEM
Yu et al. [25]	7.00%	1E − 5 mD	NA	50 mD-ft	Single porosity	GEM
Sun et al. [26]	6% (matrix), 45% (fracture)	1E − 4 mD	30 mD	100 mD	Unstructured Discrete fracture network	In-house
Xiong [27]	5.60%	3E − 4 mD	SRV 1 mD, USRV 0.1 md (intrinsic, width NA)	4000 mD, width NA	Hybrid of double and single porosity	In-house, MSFLOW_COM
Alharthy et al. [28]	5.6% (matrix), 0.22% (fracture, effective)	SRV 8E − 4 mD USRV 5E − 4 mD	SRV 0.05 mD, USRV 0.005 mD (effective)	100 mD-ft, 1E4 mD × 0.001 ft, psedudolized as 50 mD × 2 ft	Dual porosity and dual perm	GEM
Li et al. [29]	5.6% (matrix), 0.22% (fracture, UNSRV) 0.56% (fracture, SRV)	3E − 4 mD	2.16E − 3 mD 3.13E − 2 mD	100 mD	Dual porosity and dual perm	GEM
Zuloaga-Molero et al. [30]	7% (matrix)	0.01 mD and 0.1 mD	Conductivity 5 mD-ft	EDFM	GEM with EDFM	
Zhang et al. [31]	5.6%(matrix)	0.071 mD	Conductivity 4.6 mD-ft	EDFM	GEM with EDFM	
Jia et al. [16]	6% (matrix), 0.3% (fracture, effective)	0.001 mD	0.03 mD (effective)	100 mD-ft, 1E4 mD × 0.001 ft, psedudolized as 50 mD × 2 ft	Dual porosity and dual perm	GEM
Yu et al. [32]	Eagle Ford	12% (matrix)	0.0009 mD	Conductivity 10 mD-ft with number of 1800	EDFM with number of 76	GEM with EDFM
Ning and Kazemi [9]	Wattenberg Field	Geological model built in Petrel			Dual porosity	GEM

developed back to the 60 s [46] then extended to two-phase [47] and three-phase flow [48] and later the multiple interacting continua model (MINC) [49]. DP and DK share the same characteristics that fractures are expressed implicitly in the model, and the matrix is connected with fracture, the fracture is self-connected; their difference is that in the DK model, the matrix is also self-connected. On this basis, DK model is more accurate than the DP model. The dual continuum approach is a classical method to deal with natural fractures in conventional reservoirs to model the subsurface fluid transport. However, it meets several potential drawbacks in the unconventionals. One of the drawbacks is that the dual continuum approach is not able to depict the irregular and sparse fracture topologies because it is not able to define the shape and orientation of the fracture as it is expressed implicitly [50,51].

During the hydraulic fracturing process, the existing natural fracture near the wellbore is propped open (stimulated) in the stimulated reservoir volume (SRV) region [52–54], while the natural fractures outside the SRV region remains unstimulated [55–57]. Therefore, if one intends to properly capture the flow behavior in the multi-scale fracture network using the dual continuum approach, the SRV and the non-SRV regions should be differentiated regarding the fracture petrophysical properties. For instance, Alharthy et al. [28] gave the effective permeability of the natural fracture the value 0.05 mD inside the SRV region and 0.005 mD outside the SRV region. The differentiation between natural and hydraulic fractures can also be realized by the DFM method. The DFM approach can be classified as the structured and unstructured methods. In the structured method, the geometries of all the grids are the same that computational cost might be elevated because of numerous grid meshes are needed to represent the complex geometries of fractures. Recently, one algorithm of EDFM has been developed to be coupled with commercial compositional simulation software to more conveniently and efficiently model the fractured tight and shale reservoirs. EDFM is a no-intrusive method to embed fractures in the conventional simulators while keeping full functions of the original simulator. Xu et al. [58] verified the accuracy of their EDFM models by comparing the results generated from the local grid refinement (LGR) and semi-analytical solutions. Zuloaga-Molero et al. [30] applied the EDFM approach to model CO_2 huff-n-puff EOR as well as continuous flooding coupled with the mature compositional simulator GEM, regarding matrix permeability, fracture permeability and molecular diffusion. In contrast, the unstructured grids are more flexible to deal with the complex fracture network, and they are not very constrained to grid refinement. Simulations with coarsely grids are still able to obtain accurate results. For instance, Sun et al. [26] applied unstructured complex discrete fracture network to model the CO_2 huff-n-puff in the unconventional reservoirs. They obtained the conclusion that the adoption of discrete fracture yields more accurate simulation results compared with the dual continuum approach.

3. Mechanisms of gas injection

3.1. Continous gas flooding, WAG, and huff-n-puff

Gas injection can be continuous, water alternating, and cyclic, and

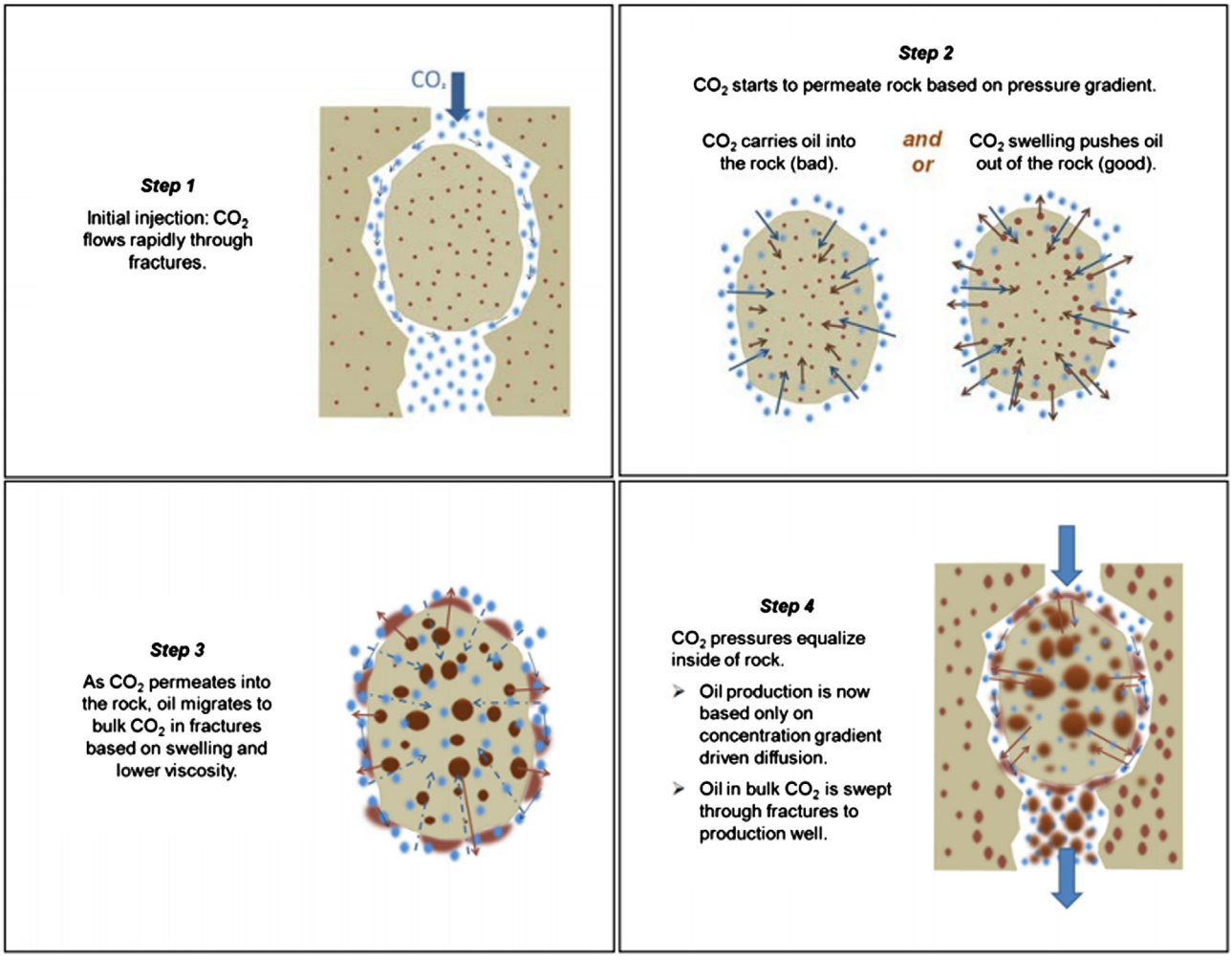

Fig. 2. Stages of CO_2 huff-n-puff in fractured oil reservoirs [62].

gas types can be nitrogen, CO_2, methane, hydrocarbon-rich gas. In the continuous gas flooding, gas is injected at the injector and oil is produced at the producer continuously. Miscibility development between gas and oil is achieved through the multicontact process, by mechanisms of vaporizing or condensing, or combination of them. The lean gas injection usually causes the vaporizing displacement that light components of crude oil vaporize into the gas phase. If the gas phase contains intermediate-heavy hydrocarbons, the condensing vaporizing displacement occurs that some heavy components of the injected gas condenses into the oil phase. In most scenarios, the displacement mechanisms are the combination of them. A successful gas injection project is aimed to increase both the macroscopic and microscopic displacement efficiency; the product of them is defined as the overall oil recovery. The macroscopic efficiency is defined as the fraction of the reservoir volume contacted by gas over the total reservoir volume. Effects of viscous fingering, unfavorable mobility ratio, gravity override, and reservoir heterogeneity all contribute to a low macroscopic displacement efficiency. The microscopic efficiency is defined as the fraction of oil displaced over the total oil contacted by gas. Not traveling enough distance to achieve multicontact miscibility and the appearance of dispersion can contribute to a low microscopic efficiently. More details involve mechanisms affecting the performance of continuous gas flooding can consult chapter 6 in the Spe Textbook by Green and Willhite [59].

Water Alternating Gas (WAG) is one widely applied injection scheme in field operations. WAG is effective because the mobility ratio between the injectant and oil is reduced and the amount of gas needs to be purchased is less. A high mobility ratio is not favorable for oil recovery because it leads to early gas breakthrough and small amount of recycled gas in the high-permeability zone. In a successful WAG project, the amount of injected water and gas, injection periods, and well controls should be optimized to achieve the maximum net present value (NPV) [60]. Advanced optimization algorithm helps achieve this goal. For instance, Chen and Reynolds [61] proposed a methodology to optimize well control and injection periods based on the Lagrangian and stochastic-simplex-approximate-gradient algorithm.

Despite that WAG has been proved to be an effective approach for improving oil recovery, gas override issue still exists in regions far away from the wellbore during gas injection period, when gas flows upward, and water/oil flow downward. This issue is more serious when large vertical heterogeneity and high-permeability channels are present in the reservoir that cause the gas override problem and subsequent early gas breakthrough. Depending on the reservoir temperature and pressure, and gas type, a large density difference between gas and water/oil also contributes to the gas override problem. In the recent years, many researchers have been advocating gas huff-n-puff process that one well acts like both injection well and production well, like the process of cyclic steam stimulation for heavy oil reservoirs, to overcome the early gas breakthrough problem for shale oil reservoirs.

Fig. 2 shows the three stages during CO_2 huff-n-puff process: huff, soak, and puff. During huff (step 1 and step 2), CO_2 is injected into the reservoir through the fractures and encompasses the matrix; the concentration gradient pushes CO_2 to permeate into the matrix. During the injection process, CO_2's carrying oil into the rock matrix from the fracture is unfavorable and pushing oil out of the matrix to the fracture is favorable for oil production. During the soak time, the well is shut in (step 3), thus "soaking stage" can also be named "shut-in stage". During this period, CO_2 swells oil and lowers oil viscosity. During puff, production well is operated constrained by the flow rate or by the production pressure, miscible or immiscible oil and CO_2 in the matrix are pushed towards the fracture by diffusion, then the bulk fluid flows back towards the production well through the fracture (step 4).

Gas continuous flooding refers to the process of injecting gas at the injection to push oil out of subsurface from the production well [63–65]. In contrast, during gas huff-n-puff or cyclic process, only one well is involved that it serves as both injection well and production well [66]. The process is composed of three stages: "huff" that the gas injection period, "soak" that the well shut-in period, and "puff" that the oil production period. In the field, the time-to-time shut-in requires interruption of the production and also requires more operations. Zuloaga et al. [67] performed CO_2 injection simulations in the Bakken formation wherein the feasibility of CO_2 continuous flooding and huff-n-puff process were tested. They found that there exists a threshold value of the matrix permeability that determines whether the CO_2 huff-n-puff or flooding is more favorable: CO_2 huff-n-puff process contributes to more oil recovery when the matrix permeability is lower than 0.03 mD [69]. Besides, they found that the presence of natural fracture has more important impact when the reservoir is performed with CO_2 huff-n-puff with a low matrix permeability.

In the real filed, one of the reasons why cyclic process is preferred over the flooding approach is suggested to be the injectivity issue. If the injectivity is too low due to the ultra-low permeability, reservoir pressure close to the injection point will be building up continuously without propagating to production well until it reaches the limit. However, based on the CO_2 pilot test in the Bakken formation, the injectivity is quite optimistic: a rate of 1 MMSCF/day had been injected into one well for 1 month and 1.5–2 MMSCF/day had been injected into the other well for 1.5 months without reaching the pressure limit. One reason by Hoffman and Evans [20] is that the wells in the pilot tests are all stimulated wells with hydraulic fracture, leading to the fact that not

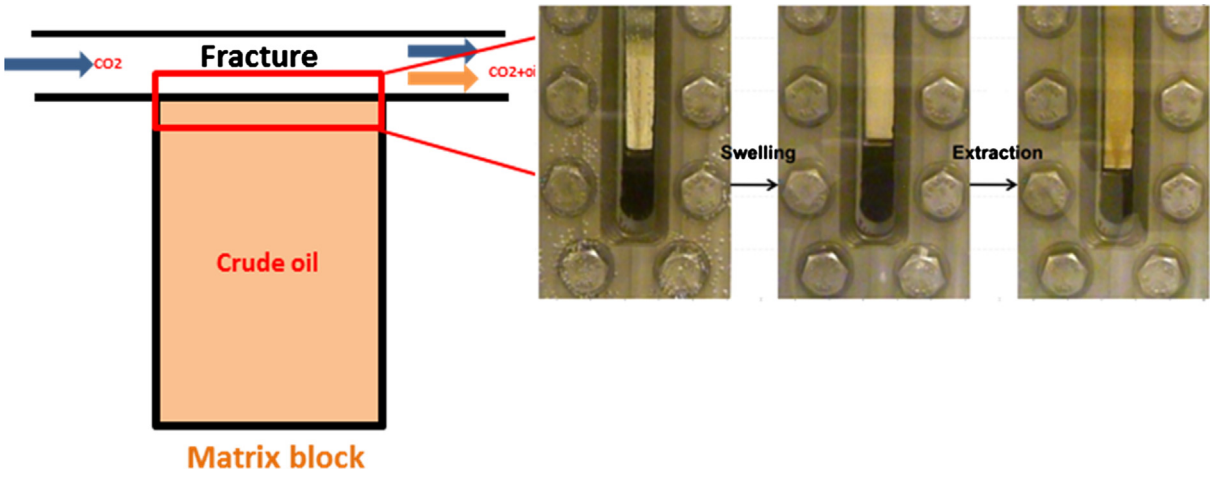

Fig. 3. Interactions between crude oil and CO_2 under different pressures. Figures from left to right indicate pressures from low to medium to high (The right figure from Tsau [72]).

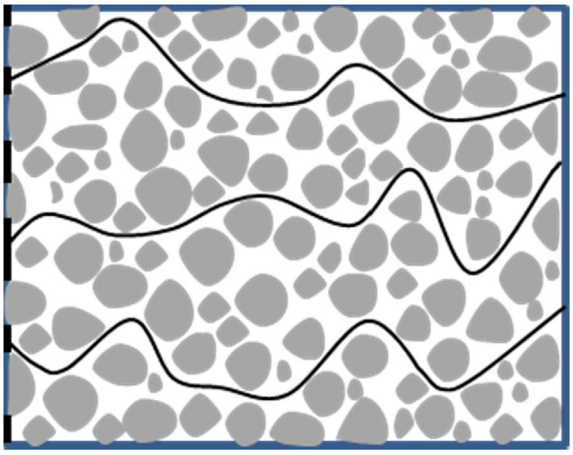

Fig. 4. Diffusion process in the porous media with effects of tortuosity and porosity.

only the gas injectivity but also the water injectivity does not seem to be an issue independent of the reservoir locations and operators. Another reason by Hoffman and Evans [68] is that the Bakken permeability and porosity in the America section are not low: the permeability is one order higher than the Canada section and the porosity is twice as much as the Canada section. From the perspective of the authors, the permeability and porosity behave high might be caused by natural fracture even though the matrix permeability and porosity are low, the measured apparent permeability and porosity are combined results of the fracture and matrix. Despite of the optimistic injectivity, the frustrating result was obtained for the gas injection tests in the Bakken. In one test, slight oil production peak appears after the well shut-in time, but the increased amount cannot compensate for the production loss in the shut-in time. In another test, no oil recovery was increased compared with the projected scenario with no gas injection. The "failure" reasons are attributed to the early gas breakthrough due to the poor conformance control, which could occur in both the injection schemes. To overcome the early breakthrough issue leading to problems of dealing with large volume of fluids and reducing oil recovered, it is necessary to shut off the high-permeability zone; conventional gel of diverting fluids are frequently used in conventional reservoirs. WAG is another option for conventional reservoirs [69–71] that the cycle time and number, inflow control values (ICV), well operations can be optimized to achieve the optimal [61]. However, the complex fracture network complicates the situation in unconventional reservoirs that mechanical approaches to isolate high-permeability zones near the wellbore region might be better of use; using unstimulated wells should contribute to better sweep efficiency, but if unstimulated, the injectivity might be a problem. In a summary for this section, we cannot over-simply say the cyclic injection is the one suitable for shale oil reservoirs based on simulation results. It still needs trial and error tests to see which injection scheme (continuous, cyclic, or WAG) is more profitable for the reservoir with the specific geological setting.

3.2. CO_2 interaction with oil in the matrix/fracture system

During the gas injection process, the depleted reservoir pressure is maintained and the miscibility between oil and gas is expected to be developed after multiple contacts. Molecular diffusion determines the rate of and the level of mixing between oil and gas. Fig. 3 shows three stages of miscibility development between oil and the injected gas from low pressure to high pressure in a visual cell. During the swelling pressure range, CO_2 dissolves into the oil phase that causes the oil volume increase. Under the low pressure, oil extraction into the gas phase is negligible that we can consider only gas diffuses into the oil phase, supported by the fact that the color of the upper gas phase does not change as pressure increase from low to medium. However, it is observed that as pressure increases from medium to high, oil volume decrease and the color of the upper gas phase turns yellow. These two facts indicate that oil has begun to be extracted into the gas phase where the pressure point exists before the pressure reaches MMP. Fig. 3 can guide us of the reservoir simulation work that unidirectional diffusion can be considered for the low-pressure gas injection and production process, but most of the time, the reservoir pressure is well above the MMP especially for the shale oil reservoir that generally has a higher temperature than conventional reservoirs. Therefore, for more realistic reservoir simulation and more accurate production forecast, we should carefully study the impact of molecular diffusion and from another point of view, it is also important to measure the diffusion coefficient, including both the binary and multicomponent diffusion coefficients in the laboratory and how we manage to upscale the diffusion coefficient from the laboratory scale to the field scale.

3.3. Diffusion in the porous media

3.3.1. The effect of porous media

Laboratory measurement of diffusion coefficient in the bulk fluid is extensive, but the measurement in liquid-saturated porous media is relatively less. The diffusion process in the porous media differs that in the bulk phase because of intrinsic properties of the porous media: tortuous and porous. Eq. (1) shows the relationship between the bulk phase diffusion coefficient, D, and the effective diffusion coefficient taking into account of the porous media, D_{eff} [73,74].

$$D_{eff} = \frac{D}{\tau^2} \tag{1}$$

where τ is the tortuosity. The tortuosity square in the denominator accounts for the twisted flow path from the inlet to the outlet (Fig. 4) instead a straight line [75].

The formation resistivity factor, F, is expressed based on Archie's law [76,77] as:

$$F = 1/\phi^m \tag{2}$$

τ can be approximated as [78]:

$$\tau = (F\phi)^{n/2} \tag{3}$$

where m and n are empirical numbers that can be assumed to be 2 and 1, respectively.

Based on the equations above, the relationship between D and D_{eff} can be inferred as [73]

$$D_{eff} = D\phi. \tag{4}$$

Eq. (4) is the one applied by Ghasemi et al. [79] to estimate CO_2 diffusion coefficient in crude oil. However, we can see that this equation is oversimplified, there are uncertain parameters as m and n. In addition, diffusion coefficient is temperature and pressure dependent. Yu et al. [25] performed sensitivity analysis of diffusivity (diffusion coefficient) in the simulation of CO_2 cyclic huff-n-puff process, and they found molecular diffusion is a favorable mechanism for oil recovery and the selection of diffusivity is important for more realistic simulation results, especially for low-permeability reservoirs. Therefore, it is crucial to perform laboratory experiments to estimate the in-situ values of diffusion coefficients.

3.3.2. The importance of molecular diffusion in the shale reservoirs

In addition to the binary and multi-component diffusion processes, the self-diffusion process is also important for gas flow in shale reservoirs. Fernø et al. [80] visualized the self-diffusion process of CO_2 in tight shale formations with dynamic CO_2 tracking and obtained the CO_2 effective diffusion coefficient from its distribution profile. In conventional fractured reservoirs, the oil recovery mechanism during gas injection includes convective flow, gravity drainage and diffusion

process. The diffusion further includes mechanical dispersion and molecular diffusion. Molecular diffusion might be insignificant in high matrix permeability reservoirs as the convective flow is the dominating mechanism of the recovery process. However, in tight reservoirs with low matrix permeability, the flow velocity is low in the matrix that the relative contribution of molecular diffusion becomes significant. In addition, the natural fracture density determines the surface area available for mass transfer between matrix and fracture [81,82]. For these reasons, molecular diffusion should be more important in highly fractured reservoir especially when the matrix permeability is very low. In a short summary for the statements in this part, (1) diffusion coefficient measurement in liquid-saturated porous media below permeability of 0.1 mD has rarely been seen in the literature that needs careful and reliable measurement especially for the multicomponent system; (2) The radial set-up has advantages over the other two set-up because it might avoid the gravity induced convective flow; (3) Grid sensitivity analysis needs to be performed in the single-porosity system when estimating the diffusion coefficient.

3.4. Empirical correlations of the diffusion coefficient

Two empirical correlations frequently applied are by Wilke and Chang and the Sigmund correlation. Wilke and Chang [83] came up with the empirical correlation to estimate the diffusion coefficient as

$$D_{ik} = \frac{7.4 \times 10^{-8}(M_{ik}^{'})^{1/2}T}{\mu_k V_{bi}^{0.6}} \tag{5}$$

where

$$M_{ik}^{'} = \frac{\sum_{j\neq 1} y_{jk}M_j}{1-y_{ik}} \tag{6}$$

where V_{bi} is the partial molar volume at the boiling pressure, which can be estimated from

$$V_{bi} = 0.285V_c^{1.048} \tag{7}$$

where V_c is the critical volume.

The diffusion coefficient is also termed as diffusivity. Sigmund [88] provided an empirical correlation to estimate the diffusion coefficient as below [85]

$$\frac{\rho_k D_{ij}}{\rho_k^0 D_{ij}^0} = 0.99589 + 0.096016\rho_{kr} - 0.22035\rho_{kr}^2 + 0.032874\rho_{kr}^3 \tag{8}$$

where $\rho_k D_{ij}$ is the product of density and diffusion coefficient, the subscript "0" indicates low-pressure. ρ_{kr} is the pseudo reduced density that can be estimated by

$$\rho_{kr} = \rho_k \frac{\sum_i^{n_c} y_{ik}v_{ci}^{5/3}}{\sum_i^{n_c} y_{ik}v_{ci}^{2/3}} \tag{9}$$

where n_c is the number of components, V_{ci} is the critical volume, ρ_k is the density.

The product of density and diffusion coefficient under low pressure can be expressed by [86]

$$\rho_k^0 D_{ij}^0 = \frac{2.2648 \times 10^{-5}T^{1/2}}{\sigma_{ij}^2 \Omega_{ij}}[1/M_i + 1/M_j]^{1/2} \tag{10}$$

where σ_{ij} is the Leonard-Jones potential parameter of i and j

$$\sigma_i = 0.1866\frac{V_{ci}^{1/3}}{Z_{ci}^{6/5}} \tag{11}$$

$$\sigma_{ij} = 0.5\sigma_i + 0.5\sigma_j \tag{12}$$

M is the molecular weight, T is temperature, is the collision integral of i and j components, which can be expressed as [84,86]

$$\Omega_{ij} = \frac{1.06036}{T_{ij}^{0.1561}} + \frac{0.193}{\exp(0.47635T_{ij})} + \frac{1.03587}{\exp(1.52996T_{ij})} + \frac{1.7674}{\exp(3.89411T_{ij})} \tag{13}$$

$$\Omega_{ij} = \frac{1.06036}{T_{ij}^{0.1561}} + \frac{0.193}{\exp(0.47635T_{ij})} + \frac{1.03587}{\exp(1.52996T_{ij})} + \frac{1.7674}{\exp(3.89411T_{ij})} \tag{14}$$

$$T_{ij} = \frac{T}{(\varepsilon/k)_{ij}} \tag{15}$$

$$(\varepsilon/k)_{ij} = [(\varepsilon/k)_i/(\varepsilon/k)_j]^{1/2} \tag{16}$$

$$(\varepsilon/k)_i = 65.3T_{ci}Z_{ci}^{18/5} \tag{17}$$

da Silva and Belery [87] improved the correlation by Sigmund [88] for the reduced density ρ_{kr} larger than 3 to avoid negative values for the diffusion coefficients.

$$\frac{\rho_k D_{ij}}{\rho_k^0 D_{ij}^0} = 0.18839\exp(3-\rho_{pr}) \tag{18}$$

It should be noticed that the empirical correlations are based on limited experimental data for limited hydrocarbon species and usually under low pressure in comparison to the very high pressure observed in the deep shale reservoirs where gas behaves more like liquid, which might cause deviation of estimation if one directly apply the Sigmund correlation and the modified version by Silva and Belery [87]. Based on the diffusion theory for low-pressure gas, the diffusion coefficient is positively correlated with temperature and inversely correlated with pressure. However, based on several experimental results, such as Renner [89] and Li et al. [90], the diffusion coefficient shows a slight trend of increasing as a function of pressure, which seems contradictory to the gained knowledge of diffusion. In a short summary for this section, molecular diffusion measurement between injection gas and oil in shales need more experiment efforts to obtain in-situ values considering the tight porous media consisting of both inorganic and organic nanopores. Empirical correlation between the bulk phase diffusion coefficient and the in-situ diffusion coefficient can be established including porosity, permeability, and tortuosity as variable parameters. Thus, more accurate reservoir modeling for oil production in shale reservoirs can be achieved with more diffusion coefficient input rather than just assumed values.

4. Heterogeneity effect and upscaling

High degree of heterogeneity exists in unconventional reservoirs, making it difficult to locate sweet spots and determine the best completion method [5]. In addition, heterogeneity also affects the production behavior of shale reservoirs significantly because of the hierarchical heterogeneity from the nanoscale organic and inorganic pores to the micro and macro fractures and the complexity of geological settings. Several researchers have been generating the stochastic field regarding permeability to explore heterogeneity-related shale oil production behavior.

4.1. Heterogeneity/correlation length effect (matrix) on gas injection performance

Chen et al. [22] generated two-dimensional permeability field to investigate effects of heterogeneity and correlation length on primary oil recovery and CO_2 huff-n-puff performance. Correlation length is a parameter characterizing the distance scale between two points that the correlation function disappears [91]. The computation domain is illustrated in the red rectangle of Fig. 5 where the hydraulic fracture was located in the middle the region. Single-porosity model was applied in their compositional model UT-comp that only Darcy flow was considered. The degree of heterogeneity was evaluated by the

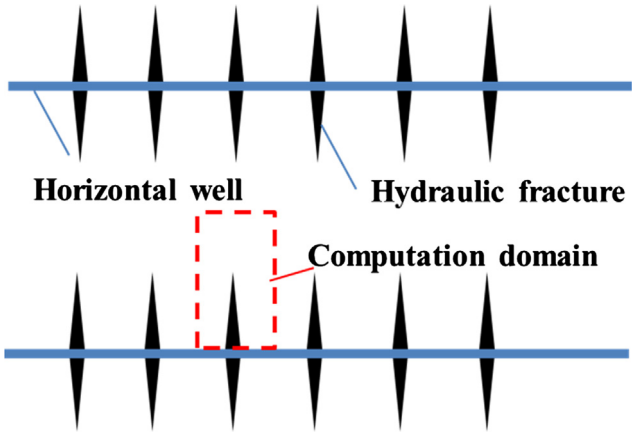

Fig. 5. Top view of computation domain in the work by Chen et al. [22].

Dykstra–Parsons variation coefficient [92–94], V_{dp}, which is defined as

$$V_{dp} = \frac{k_{50} - k_{84.1}}{k_{50}} \tag{19}$$

where k_{50} is the median in the permeability distribution spectrum, and $k_{84.1}$ is the median added with one standard deviation. Mean value of permeability of the matrix was set to be 0.01 mD, which was the same in all simulation scenarios. Dykstra–Parsons coefficient varied from 0.3746 to 0.7313. The correlation lengths in the x and y directions in the base cases were set to be 40 ft, and different values were applied for the later sensitivity analysis. The homogeneous scenario was also simulated for comparison purpose. In their simulations, the production period was divided into two stages: primary production and cyclic CO_2 injection. Primary production lasted for 300 days. It was found that $(1 - r/r_m)$ is negatively and linearly related with Dykstra–Parsons coefficient in the semi-log plot and insensitive to the correlation length effect, where r is the recovery factor at a certain time, and r_m is the recovery factor at the end of production. During the CO_2 huff-n-puff process, the schedule of 30 days' injection-10 days' shut-in-100 days' production was repeated for 1000 days. The primary production also lasted for 1000 days in comparisons with the two-stage process. Based on their simulation results, the oil recovery factor by the CO_2 huff-n-puff is lower than that by simply primary production because during the CO_2 injection and soaking periods oil is not produced, even the peak of the production rate after soaking is very high. Besides, they found that no incremental oil recovery if the soaking time increases from 10 days to 20 days because of the limited CO_2 dissolution amount in the oil and small CO_2 flow back rate. Their work revealed the importance of taking account into the heterogeneity effect in the near-wellbore region in both primary depletion and huff-n-puff process.

4.2. Heterogeneity/correlation length effect (natural fracture) on huff-n-puff performance

Inspired by the work by Chen et al. [22], Jia et al. [16] performed a study of field-scale heterogeneity effect on primary and huff-n-puff processes with a focus on the role of molecular diffusion. Considering the importance of natural fracture system, the natural fracture permeability was set as the variable instead of the matrix permeability. A horizontal well with 12-stage hydraulic fracturing was located in the middle field. Fig. 6 shows the natural fracture permeability distribution patterns with the correlation length varying from 50 ft to 3000 ft while keeping the Dykstra–Parsons coefficient at 0.64 and the mean value at 0.03 mD. The Dykstra–Parsons coefficient varied from 0.40 to 0.78 in other series of scenarios. Based on the primary oil recovery results, it was found that the heterogeneity hampered oil recovery performance, but as the correlation length increase, the heterogeneity-induced negative effect was relieved. The CO_2 huff-n-puff process started when the primary recovery factor reached 3%. Two schemes were applied: multi-cycle scheme with fixed 10 days' injection-10 days' soaking-100 days' production scheme and the single-cycle scheme with fixed CO_2 injection amount equals 0.3% of reservoir volume which needed about 1000 days' injection. Different effects of correlation length were observed in the multi-cycle and single-cycle scheme: long correlation length was more favorable while short correlation length was more favorable for oil recovery performance. CO_2 injectivity as a function of time could explain this behavior: a long correlation length is more favorable in the long term while a short correlation length is more favorable in the short term. Molecular diffusion was taken into account of the simulation by the Sigmund correlation. It was found that if diffusion

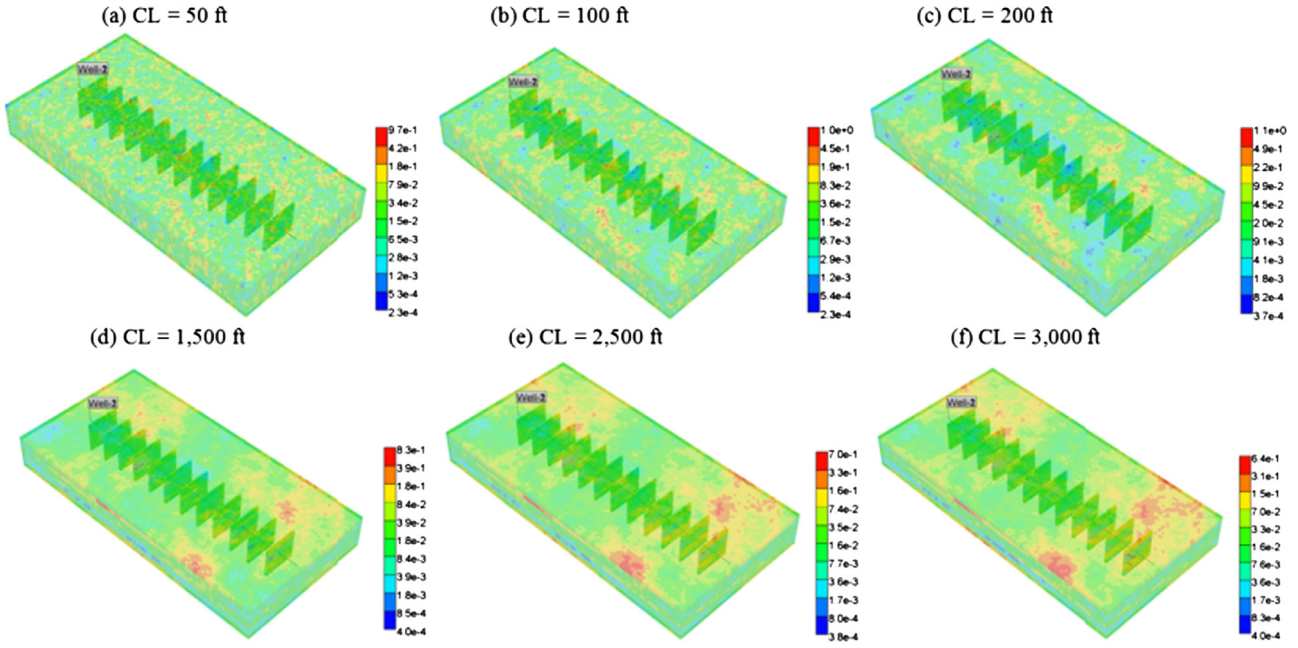

Fig. 6. Natural fracture permeability distribution patterns in six simulation scenarios, Dykstra–Parsons coefficient is 0.64 in all the six scenarios. Correlation length varies from 50 ft to 3000 ft from (a) to (b), the grid size is 50 ft in the x and y directions [16].

is not considered, the reservoir pressure would increase after the soaking period; if diffusion is considered, the reservoir pressure would decrease. The suggested reasons are that the oil swelling upon contacting with CO_2 causes the pressure increase in the system with no-flow boundary conditions; when molecular diffusion is considered, oil vaporization into CO_2 and CO_2 dissolution into oil is more enhanced accelerating the mixing degree between the two phases, causing reduction of the interfacial tension and leading to the slight decrease of the system pressure. During the huff period, it was found that molecular diffusion reduces the gas oil ratio (GOR) and thereby extends the lifetime of the shale oil reservoirs. The relationship between molecular diffusion, heterogeneity and correlation length is complex: a low degree of heterogeneity is unfavorable to oil recovery, but a high degree of heterogeneity shows a favorable effect at a long correlation length when the molecular diffusion is taken into account. It revealed that in the complex shale reservoirs, natural fracture system is essential for the development of shale reservoirs, which should be characterized through an integrated petrophysical approach prior to drilling and stimulation.

4.3. Methodology of upscaling gas injection in shale reservoirs

For field-scale simulations, the size of grid blocks is preferred to be as large as possible to save computation time. However, the large block might cause inaccurate modeling result because of involvement of molecular diffusion, such as in the miscible gas injection process. The reason is that that the molecular diffusion is scale dependent because the contact area increase as the fluid travel distance increases. Garmeth and Johns [95] performed the pioneer upscaling work to upscale continuous gas miscible flooding considering the degree of reservoir mixing caused by dispersion. They constructed two-dimensional conceptual heterogeneous models for reservoir simulations. They developed two functions to investigate upscaling of the local dispersity. One is based on first contact miscible (FCM) simulations to investigate how six factors affect the degree of reservoir mixing as Dykstra–Parsons coefficient based reservoir heterogeneity, x- and y-direction correlation length, mobility ratio, aspect ratio, and the number of dispersion. The other function is to investigate the effect of the ratio between traverse and longitudinal velocities. They concluded that the local dispersity is different in different scales because of the varying gas/oil contact areas versus traveling distance and influenced by all the six factors investigated. The overall dispersion is the total effect of reservoir dispersion and simulator dispersity that should be the same for small and large simulation blocks to obtain accurate reservoir recovery results. They also observed that higher reservoir heterogeneity and longer longitudinal correlation length are more favorable for oil production, which well explained the finding that oil recovery is higher as heterogeneity and correlation length increase during the scheme of gas huff-n-puff in the work by Jia el al. [16].

It is difficult to upscale flow properties and production behaviors in the complex shale reservoirs from pore scale to core scale, and it is even more challenging from core scale to field scale. Li and Sheng [96] developed a methodology to generate type curves to correlate the oil recovery factor with the self-defined dimensionless time with different scales for the gas injection EOR process. Oil recovery efficiency by huff-n-puff was expressed as using self-defined dimensionless pressure. Based on the generated types curves they concluded that to increase the oil recovery efficiency, the operation time of the gas injection should be reduced. They used pressure depletion data of primary production to validate their model considering the limited field data of real huff-n-puff field operations. The upscaling results should be of more significance if molecular diffusion is considered, and if field operation data during gas injection in shales are available.

5. Nanopore effect on the phase behavior

5.1. Approaches to estimating phase behavior alternation due to the pore confinement effect

Based on the International Union of Pure and Applied Chemistry (IUPAC) classification, pore with sizes smaller than 2 nm, 2 nm to 50 nm, larger than 50 nm are termed as micropore, mesopore, and macropore, respectively. The size of throat connecting adjacent pores are even smaller than the pores themselves. In tiny pores, the phase envelope of reservoir fluids might shift because hydrocarbons are under metastable state that the bubble point might be suppressed and dew point might be increased [97–100]. This feature is considered to be more important for gas condensate reservoirs when the pressure decline crosses the phase envelope. Zarragoicoechea and Kuz [101] derived empirical correlations for shifts of critical properties between the bulk phase and pore-confined phase, with assumptions that no adsorption occurs.

$$\Delta T_c = \frac{T_c - T_{cp}}{T_c} = 0.9409\frac{\sigma}{r_p} - 0.2415\left(\frac{\sigma}{r_p}\right)^2 \tag{20}$$

$$\Delta P_c = \frac{P_c - P_{cp}}{P_c} = 0.9409\frac{\sigma}{r_p} - 0.2415\left(\frac{\sigma}{r_p}\right)^2 \tag{21}$$

where T_c and P_c are the critical temperature and critical pressure in the bulk phase, respectively, T_{cp} and P_{cp} are critical temperature and pressure with the pore confinement, σ is the collision diameter also known as Lennard-Jones size parameter, and r_p is the pore size. It is observed that the ratio of properties' change is a function of the ratio of the molecule size to the pore size. Experimental data points of the critical temperature of different gases are compared against their model as in Fig. 7. It can be found that very good agreement is achieved with small size ratios, while the deviation at larger size ratios might be attributed to the multilayer adsorption.

Based on the van der Waals equation of state, Singh et al. [102] applied improved Monte Carlo simulation to explore pore confinement effect on properties of pure hydrocarbons. They found that the pore size and surface characteristics of the pore wall affect critical temperature, critical pressure and density of the hydrocarbons. The surface tension between the liquid and vapor phases is suppressed due to the confinement effect.

Devegowda et al. [103] (Table 3) extrapolated simulation results by Singh et al. [102] and provided correlations between confined critical properties and molecular weight, as well as the viscosity and compressibility factor changes due to the confinement. The Table below

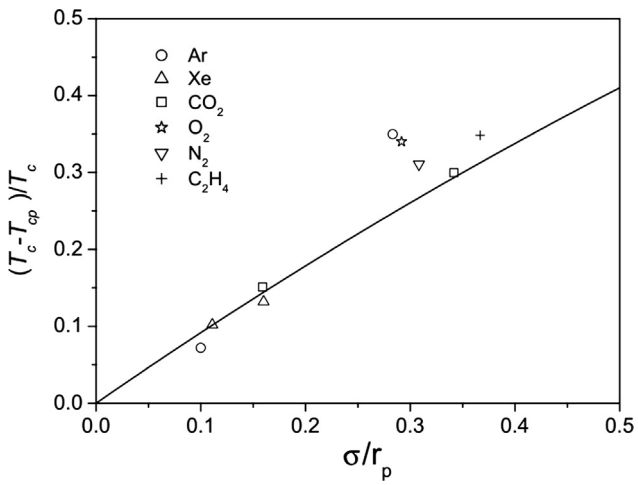

Fig. 7. Shift of critical temperature as a function of the size ratio, experimental data and the model result [101].

Table 3
Shifts of critical properties in pores with different diameters [103].

	2 nm	4 nm	5 nm
ΔP_c	0.085ln(MW) − 0.0693	−0.085ln(MW) + 0.1193	−0.077ln(MW) − 0.041
ΔT_c	0.0636 $MW^{0.2129}$	0.0229 $MW^{0.2319}$	0.0229 $MW^{0.241}$

shows these correlations in pores with diameters of 2 nm, 4 nm, and 5 nm.

Ma et al. [104] and Jin et al. [105] also derived empirical correlations based on different size ratios, according to the van der Waals equation of state.

$$\Delta T_c = \frac{T_c - T_{cp}}{T_c} = 0.6\frac{2r_p}{\sigma} \leq 1.5 \tag{22}$$

$$\Delta T_c = \frac{T_c - T_{cp}}{T_c} = 1.1775\left(\frac{2r_p}{\sigma}\right)^{-1.338}\frac{2r_p}{\sigma} \geq 1.5 \tag{23}$$

$$\Delta P_c = \frac{P_c - P_{cp}}{P_c} = 1.5686\left(\frac{2r_p}{\sigma}\right) \tag{24}$$

Fig. 8 shows the modified flowchart by Jin et al. [105] for the flash calculation.

The above methodology is based on modifying critical properties of components in the flash calculation. Li and Sheng [106] applied the approach proposed by Ma et al. [104] and Jin et al. [105] to analyze the Wolfcamp multicomponent crude oil. Their results show that the bubble point decreases by 17.3% and 63.8% in a pore with sizes of 10 nm and 1.5 nm, respectively. The interfacial tension reduces as pore size reduces especially when the pore size is smaller than 10 nm. The well lifetime is extended because of the reduced capillary pressure in nanopores.

In addition, the involvement of capillary pressure in the flash calculation is categorised as the second approach, which is frequently neglected in the conventional reservoirs. One of the representative work using this approach is by Nojabaei et al. [107]. The pressure across the interface between the vapor and liquid is expressed as:

$$P^v - P^L = p_c \tag{25}$$

where P^V is the vapor pressure and P^L is the liquid pressure. The capillary pressure, P_c, is expressed using the Young-Laplace equation

$$p_c = \frac{2\sigma_F}{r_p} \tag{26}$$

Across the interface fugacity of two phases are equal

$$f_i^L = f_i^V \tag{27}$$

At the dewpoint the equations below are established

$$f_i^L(T, P^L, x_1, x_2 \ldots x_{N_c}) = f_i^L(T, P^L, z_1, z_2 \ldots z_{N_c}) \tag{28}$$

$$\sum_{i=1}^{N_c} x_i = 1 \tag{29}$$

where x_i indicates the fraction of i in the liquid phase, and z_i indicates the global fraction of i, and N_c is the number of components.

At the bubble point, the equations below are established

$$f_i^V(T, P^L, y_1, y_2 \ldots y_{N_c}) = f_i^L(T, P^L, z_1, z_2 \ldots z_{N_c}) \tag{30}$$

$$\sum_{i=1}^{N_c} y_i = 1 \tag{31}$$

The interfacial tension between the two phases is expressed based on the Macleod and Sugden correlation [108] as

$$\sigma_F = \left[\sum_{i}^{N_c} \chi_i (x_i\rho^L - y_i\rho^V)\right]^4 \tag{32}$$

where χ_i is the parachor coefficient, ρ^V and ρ^L are densities of vapor and liquid, respectively. Nojabaei et al. [107] performed a sensitivity analysis by increasing the parachor number with 10%. They observed that the reduction of bubble point pressure of C1/C6 mixtures increases from 74 psi to 123 psi, revealing the significance of an accurate parachor number for the accuracy of the phase behavior prediction.

Fig. 9a shows the bulk and shifted phase envelopes for two-phase mixtures. It could be observed that as a whole, the confinement has larger effect on the bubble point than the dew point. The bubble points are suppressed in all curves but the dew points are not consistent, Fig. 9b directly plots the differences for the bubble point and dew point pressures. The bubble point difference is larger under low temperature and becomes zero approaching the cricondentherm; the dew point difference is negative under pressure lower than the cricondentherm but positive under pressure higher than the cricondentherm, and both of them do not change at the critical point because the interfacial

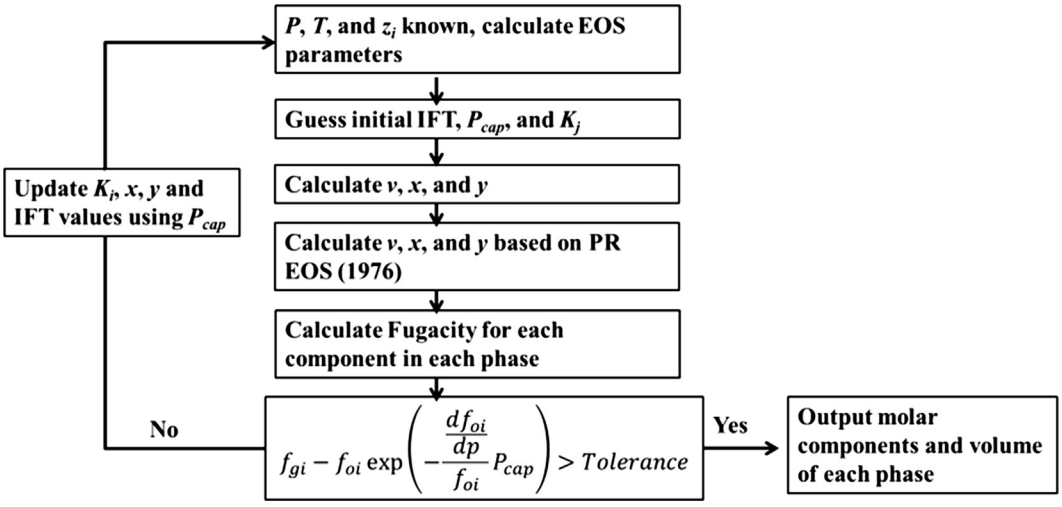

Fig. 8. Flowchart of the modified flash calculation by Jin et al. [105].

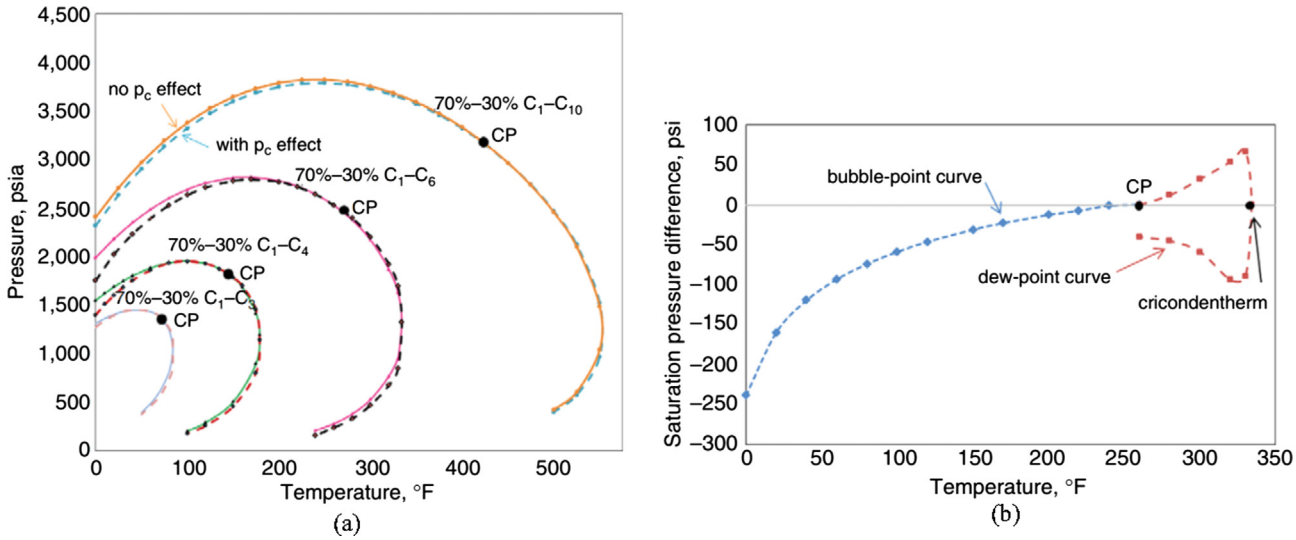

Fig. 9. (a) Phase envelopes' changes for mixtures of C1/C10, C1/C6, C1/C4, and C1/C3 with a pore radius of 10 nm. (b) The difference of saturation pressure between the bulk phase and confined phase for the C1/C6 mixture [107].

tension is zero. Nojabaei et al. [107] also pointed out that due to pore size heterogeneity, the different extent of bubble point suppression occurs in the reservoir. Thus two-phase forms in some pores while in some pores it remains a single phase. Below the bubble point, pressure gas flow becomes continuous in the reservoir only upon reaching a critical point, due to the uniformity of gas saturation in tiny pores, the critical gas saturation is reasonable to be higher in shale reservoirs. This observation might well explain the discontinuous GOR in some wells of the Bakken formation. Nojabaei et al. [107] performed history matching of the bottom hole pressure and gas flow rate; a better matching result was obtained with the modified phase behavior. Haider et al. [109] applied the similar approach as Nojabaie et al. [107] and incorporated the modified phase behavior files in Automated Differentiation based General Purpose Research Simulator (AD-GPRS) of Stanford University to study the hydrocarbon production behavior in the Bakken formation. They obtained several novel findings: (1) the presence of shifted phase envelope causes the oil production to increase but the gas production to decrease; (2) given a realistic pore size distribution, 10% increase of condensate and 4% reduction of gas are observed; (3) heavier hydrocarbon has larger effect altering the phase envelope in the multiple composition systems; (4) and proper treatment of the fracture model and configuration is crucial to analyze the shifted phase and the associated production behaviors.

Wang et al. [110] extended the stability test to include the capillary effect. The stability criterion is met when

$$\sum_{i}^{M} y_i[\ln f_i(y) + \ln \varphi_i(y) - \ln z_i - \ln \varphi_i(z) + (\ln P^V - \ln P^L)] \geq 0 \tag{33}$$

where y and z are fractions in the incipient and original phases, respectively, and $f(y)$ and $f(z)$ are the corresponding fugacities. φ is the fugacity coefficient. The term (lnP^V-lnP^L) accounts for the effect of capillary pressure caused by the tiny pores. Different from Nojabaei et al. [107], Wang et al. [110] applied the Leverett J-function to estimate the capillary pressure.

Jin and Firoozabadi [111] applied molecular simulation and thermodynamic modeling to model fluid phase behavior in nanopores with considering adsorption. In addition to the adsorption on the pore surface, molecular simulation also captures the phenomenon of dissolution into shale minerals. For pore size larger than 10 nm and smaller than 100 nm, they observed a decrease in the bubble point pressure and lower dewpoint pressure and an increase in the upper dewpoint pressure. They also found that gas solubility in water and hydrocarbon increases because of the presence of the curvature between two phases. For pore size smaller than 10 nm, they found that using the modified equation of state in such tiny pores has no theoretical basis because the liquid density is underestimated and the erroneous prediction of liquid dropout in gas condensate reservoirs. They recommended that application of density functional theory (DFT) [112,113] and Monte Carlo simulation [114] can lead to a more realistic result, which depends heavily on the pore size distribution (PSD), kerogen chemical composition, and rock chemistry. They reported saturation pressure and critical properties increase due to the pore confinement. Wang et al. [115] explored pure hydrocarbon component of n-octane flow behavior in silica (inorganic) nanopores using molecular dynamics. They demonstrated that in inorganic slits with an aperture larger than 3.6 nm, properties of viscosity, self-diffusion and density behave like that in the bulk phase. In slits with an aperture larger than 1.7 nm, a combination of continuous flow, slip flow, and apparent viscosity is able to describe the fluid transport properly. Slip length, which is used to quantify the magnitude of slip slow, decreases as the aperture increases. However, when the aperture is very small, i.e., 5.24 nm, the contribution of slip flow and the apparent viscosity are also very important to the total flux. They stated that empirical correlations of the pore size, pressure gradient, and temperature dependent slip length and reduced viscosity can be developed based on results of molecular dynamic simulations readily for the application of determining shale permeability. Wang et al. [116] also explored alkane and supercritical CO_2 transport behavior in organic pores. They found that CO_2 has more adsorption capacity than methane and octane, and hydrocarbon fluids have more adsorption capacity in organic pores than in inorganic pores, depending on mineralogy of shales. The flow capacity of supercritical CO_2 is more than that only considers the slip flow, due to the small flow friction between solid and fluid at the graphite surface. Also, apparent viscosity is also proposed to be integrated into the framework of upscaling fluid flow in the shale matrix and estimating shale permeability. In both organic and inorganic pores, it is found that increasing temperature reduces adsorption profile and increases flow capacity, therefore heating up the reservoir to recover oil should be a feasible approach.

In summary for this section, to simulate oil production process when the reservoir pressure crosses the phase envelope, the pore confinement effect should be emphasized for accurate reservoir simulations. Modification of the current EOS is one approach. On the other hand, molecular simulations based on investigating phenomena at the atom level might be a more reliable approach that captures more realistic physical and chemical processes, such as gas dissolution into shale

minerals.

5.2. Pore confinement effect on oil recovery performance

It is seen from Section 5.1 that it is complex to model the nanopore effect, and there exists debate between different theories, and seldom, the proposed model and simulation results are validated by solid experimental data. Nevertheless, the consensus is that as long as the reservoir pressure crosses the phase envelop, “abnormal” phenomenon occurs that the bubble point is suppressed and the dew point is suppressed or elevated, Several researchers applied methodologies above to include the nanopore effect in their simulation to analyze and predict primary production, gas injection and oil production behaviors. Xiong et al. [27] improved their in-house compositional simulator taking into account of both the pore confinement effect and the rock compaction effect which is induced by the fluid extraction from the reservoir. Both porosity and permeability decrease as the effective stress increases for the liquid system or high-pressure gas system because the pore size is reduced [117–119]. They found that the bubble point suppression is enhanced considering the compaction (geomechanical) effect, resulting in more liquid phase rather than two phases in the subsurface. The capillary pressure was taken into account in the vapor liquid equilibrium (VLE) calculation which is also stress-dependent. Rock compaction hampers the performance of shale oil reservoirs because porosity and permeability both are reduced, while the impact of the capillary pressure becomes more significant because of the smaller pore size. Zhang et al. [120] explored the primary production based on the Middle Bakken formation with a commercial black oil simulator using the altered PVT data file. The modified Peng-Robinson equation with considering the capillary pressure and the Macleod-Sugden relation was used to estimate the interfacial tension. The properties change by the nanopore effect for the black oil model include the formation volume factor, solution gas ratio, and oil viscosity, which vary below bubble point pressure and stay the same above the bubble point pressure. The formation volume factor and solution gas ratio are enhanced, and the oil viscosity decreases due to the pore confinement. Given a randomly distributed pore size distribution, the oil production and gas production are enhanced by 7% and 8% after 30 years, respectively. Zhang et al. [120] included the shifted critical properties in the equation of state. They found that the combined effects of nanopore effect, molecular diffusion, and fracture impaction effect lead to an increase of 3.8% of oil production.

6. Experimental studies

6.1. Methods to measure the diffusion coefficient

There have been numerous studies regarding the measurement of diffusion coefficient in the bulk phase [121–125]. However, studies taken place in the porous media is relatively limited. Based on a comprehensive literature survey, three approaches were applied to measure diffusion coefficients in liquid-saturated porous media, as illustrated in Fig. 10. Fig. 10a shows the schematic that the gas is located in the upper phase and the liquid-saturated porous media is in the lower phase. The gas phase can be controlled either with a constant volume that the upper part of the cell is fixed or a constant pressure that by a piston with fixed hydraulic force connected. Initially, gas and oil are under the identical pressure. For the scenarios that the volume of the gas phase is fixed, pressure declines because of the chemical potential gradient between the two phases. The three-dimensional configuration of the experiment is easy to be constructed to simulate the pressure decline process. The rate of the pressure decline is closely related to the magnitude of the diffusion coefficients that can be set as tunable parameters to history match the recorded pressure profiles. The representative work is by Ghasemi et al. [79]. They studied diffusion coefficients between CO_2 and live oil/stank oil with the single-porosity model in the commercial software Eclipse. For the scenario that the pressure of gas phase is fixed, it is not convenient to directly apply the commercial software to simulate the process as the volume of the gas phase is dynamically changing. However, the mass of the injected gas is a function of time which is also related to the diffusion coefficient. As pointed out by Renner [89], pressure decline by the configuration of Fig. 10a is contributed by both convective flow caused by gravity drainage and molecular diffusion supported by the fact that the estimated diffusion coefficient is smaller if the core is placed horizontally instead of vertically. In other words, pressure declines faster compared with the scenario that if only molecular diffusion is present in the model. The liquid-saturated core is placed in the center of the core cell that the gas phase is saturated in the surrounding annulus initially in Fig. 10b. Similar to the constant volume approach in Fig. 10a, in Fig. 10b, the pressure decline profile can be used to estimate the diffusion coefficient. However, because of the difference of the configurations, most of the fluid would accumulate at the right bottom corner and fluid moves upward, therefore, the gravity drainage phenomenon is not important in it, and thus, the pressure decline will be mostly contributed by the molecular diffusion. This is true with CO_2 because of the density of liquid/CO_2 mixture is denser but not necessarily true with other gases.

Ghasemi et al. [79] used the single-porosity model to match the pressure decline curves obtaining vectors of diffusion coefficients in oil and gas phases. They did not report the grid sensitivity result for their values. As pointed out by Eide et al. [126], it should be careful to apply the laboratory result for field production simulation. In the single-porosity model, fractures are expressed explicitly, and different refinement of the grid might generate different matching results. A practical approach is obtaining diffusion coefficients with increasing number of grid blocks; then the obtained diffusion coefficient is plotted as a function of the reciprocal of the grid number. The intercept can be considered for the value applied for dual continuum reservoir simulation. The reason is that in the dual continuum approach which is frequently used to describe fractured porous media, a gird cell actually represents numerous blocks that every block is under the same

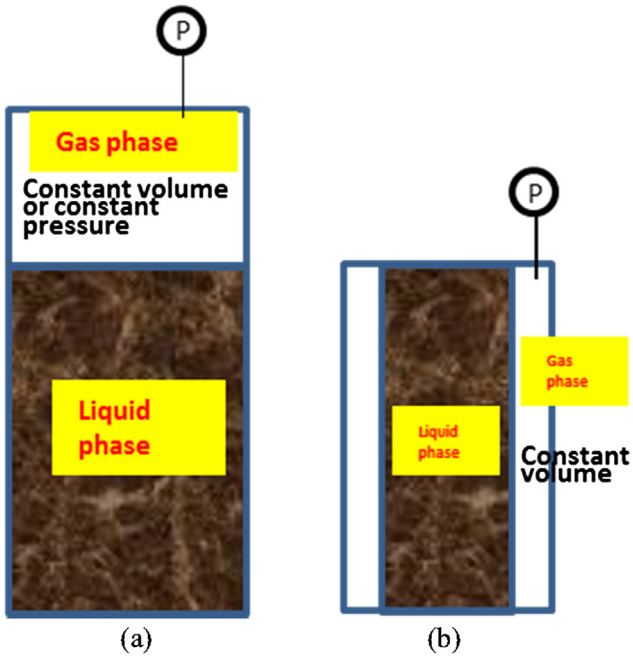

Fig. 10. Three approaches available in the literature to measure the diffusion coefficient in liquid-saturated porous media: (a) represents two approaches, the upper gas phase is injected either with the constant-volume or constant-pressure schemes; (b) represents the approach that the liquid-saturated porous media is located at the center of the core cell, and the gas is saturated in the annulus [79,89].

unequilibirum state condition surrounded by the fracture [87], forming numerous matrix/fracture units. Therefore, the flux at the interface between the matrix and fracture could be expressed from a single matrix-fracture unit where the flux can be calculated based on Fick's law in the finite difference algorithm. For example, the flux between the components of i and j caused by molecular diffusion is expressed as [127]

$$J_{ijk} = -(\phi S_j D_{ij}. F_{jk}.)\nabla(\rho_j X_{ij}) \quad (34)$$

where ϕ is porosity, S_j is the saturation of component j, k indicates the flow direction, D is the diffusion coefficient, F_{jk} is the tortuosity for the j species in phase k, $\nabla(\rho_t X_{ij})$ indicates the gradient of component i in phase j in k direction.

Besides the conventional constant volume and constant pressure methods, advanced technologies such as the Magnetic Resonance Imaging (MRI) and Nuclear Magnetic Resonance (NMR) can be utilized to measure the diffusion coefficient as well. Teng et al. [128] applied MRI to measure the diffusion coefficient between CO_2 and n-decane in glass beads. The MRI methodology is based on that the apparatus signal strength is proportional to the proton density, and thus CO_2 concentration is obtained. Based on the CO_2 concentration variation rate, the diffusion coefficient is estimated. They found the diffusion coefficient is higher under higher pressure and when larger glass beads were used. The NMR technology is based on that the relaxation spectra of two kinds of fluids to measure the diffusion coefficient is different. It has been applied to measure diffusion coefficient between the solvent and heavy oil in oil sands. Afsahi and Kantzas [129] applied NMR to measure diffusion coefficients between five solvents and three heavy oil samples from analytical solutions. They found that the diffusion coefficient in the bulk phase is higher than that in the porous media and higher when the heavy oil viscosity is lower.

6.2. Gas injection experiments in shales

Laboratory core-scale gas injection in tight cores to improve oil recovery has been performed in several research groups in recent years. Fig. 11 shows the basic components for the gas extraction or huff-n-puff experiment in most of the literature. The core is placed in the center of the cell. Either core saturated with the oil or the preserved core is used. The empty space is simulating the fractures. Tovar et al. [130] filled the empty space with glass beads that should be more representative of the subsurface because the proppants are embedded in the hydraulic fractures. Back pressure regulators are sometimes installed after the core cell to control the production pressure which is more like the field operation scenario. Otherwise, the ambient pressure is applied as the bottom hole pressure.

Tovar et al. [130] used two preserved sidewall cores initially saturated with crude oil to observe the CO_2 huff-n-puff performance, which is the first of using large-size preserved core-scale samples for such experiment, to the best of our knowledge. Permeability and porosity of the sidewall cores were not reported, which was because cores were initially saturated with crude oil. Lacking such data, they assumed values of the porosity of the cores from 0.3% to 0.6% to estimate the oil recovery factor and assumed the water saturation varied from 0% to 30%. Temperature they applied was 150 °F. They performed the experiments under two different pressures: 3000 psi and 1600, and later computed tomography (CT) images were applied to interpret fluid density change based on the CT number. One feature of their experiment was that glass bead was filled in the annulus mimicking proppants embedded in the hydraulic fracture, which was closer to the real subsurface scenario compared with the set-up that the annulus is empty. One more feature was that they applied BPR to control the effluent pressure instead of blowing down the system pressure directly, which was more like the real field operation of keeping constant bottom hole pressure. The color of recovered oil contained in a graduated cylinder was lighter than that observed in the field indicating CO_2 extracts light components of the crude oil. For the 3000 psi scenario an increasing trend of the system pressure was observed and for the 1600 psi scenario and a decreasing trend was observed. The CO_2 densities under 3000 psi and 1600 psi were estimated to be higher and lower than the oil density, respectively, the suggested reason is that CO_2 dissolution into oil is the main mechanism controlling the system density. An important discovery made is that the core weight was heavier after performing the experiments under 3000 psi which is believed to be above the minimum miscible pressure. It was suggested to be caused by the CO_2 adsorption onto the pore surface.

Song and Yang [131] performed CO_2 huff-n-puff experiments in three scenarios under different operation pressure: 1,015.26 psi, 1,348.85 psi, and 2,030.53 psi, representing immiscible, near-miscible, and miscible conditions, respectively. The temperature they applied was 145.4 °F. In the immiscible scenario, gas injection continued for 3 h, the system soaked for 6 h, and oil production lasted for 1 h. Totally six cycles were performed. During the soak period for the six cycles, the system pressure decrease during the soaking period increased in the first cycle then decreased in the following cycles. The reason is that from the first cycle to the second cycle, CO_2 injection amount and its dissolution amount increases; for the other cycles, less and less and remaining oil is left in the system so that the extent of pressure decreases is dampened. The immiscible CO_2 huff-n-n-puff recovered 42.8% oil which was even less effective than the waterflooding. In the near-miscible scenario, four cycles were performed. It was found that the period recovers the most oil occurred in the first two cycles. The

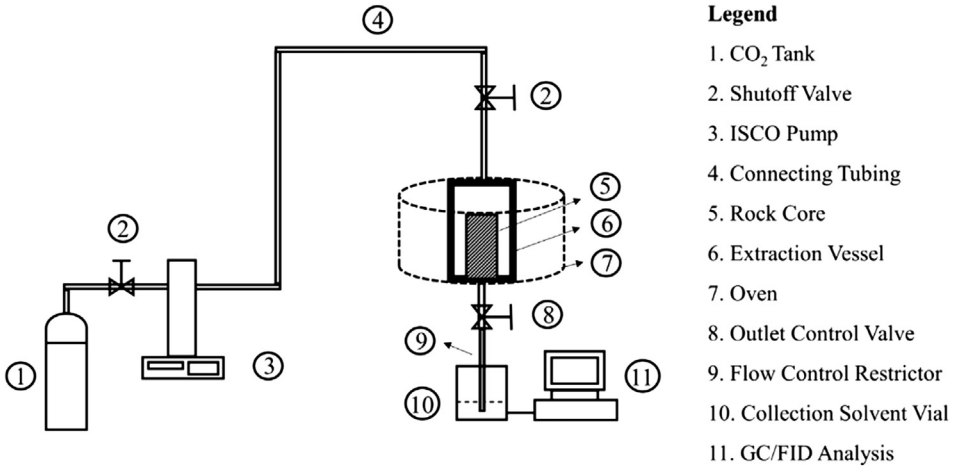

Fig. 11. Schematic experimental set-up for the CO_2 extraction experiment [124].

total oil recovery reaches 63% which is an improvement compared with the immiscible scenario, due to the larger dissolution of CO_2 by the higher injection pressure. In the miscible scenario, the oil recovery factor reached 61%, which is in fact slightly less than the near-miscible scenario which is 63%, indicating that injection pressure higher than the MMP might not be necessary as higher pressure means higher operational cost. It is worthy to mention that the porosity of their four cores ranges from 18.6% to 23.1%, and the permeability ranges from 0.27 to 0.81. These cores might not be representative for ultra-low permeability and porosity of the characteristic of shale reservoirs.

Jin et al. [132,133] collected 21 preserved small samples from Lower Bakken, Middle Bakken, Upper Bakken, and Three Forks with 1.1-cm diameter and 4-cm length to perform the extraction experiment using CO_2 under the temperature of 230 °F which is the temperature for the Bakken play. The injection pressure was maintained at 5000 psi and the production time lasted for 24 h. The flow rate was controlled at a small flow rate of 1.5 cm^3/min at the outlet to relieve pressure in the cell to ambient pressure. Because the flow rate was so small that it could be considered that the pressure-difference driven convective flow was negligible, hence the diffusion mechanism dominated the flow process. After the oil recovery experiment, the core samples were crushed into powders, and the remaining oil was collected to measure the volume and the corresponding recovery factor. Very high recovery factor (maximum 99%) was obtained for the samples from the Middle Bakken and Three Forks; about 60% recovery factor was obtained for the samples from the Upper Bakken and the Lower Bakken (Fig. 12). They applied the analysis of variance (ANOVA) and relative importance analysis (RIA) to find correlations between various factors with the oil recovery performance. Their results show that the percentage of TOC is the most influencing factor (Table 4, Fig. 13). Two reasons are provided as follows. (1) Kerogen makes the pore surface oil-wet. Thus CO_2 is difficult to extract oil from inside. (2) Pore size in kerogen is generally smaller than that in the non-organic matrix, making the capillary pressure too large for oil to be extracted. The porosity and permeability are the two least important factors. In conventional reservoirs pore size is large, convective bulk flow is the dominating flow mechanism. Thus the porosity and permeability were important reservoir properties controlling oil recovery rate. In this experiment, the flow rate is minimized so that the diffusion process is the dominating. Therefore, porosity and permeability are no longer important.

Fig. 14 shows the matrix/fracture system in the formation with one multi-stage hydraulic fractured horizontal well. The area in the red rectangle can be regarded as one unit. Based on the comprehensive literature review of gas injection experiment in shales, it is found that

Table 4
ANOVA analysis result for impacts of various factors affecting oil recovery [132].

Factor	Sum of Squares	Mean Square	F-statistic	P-value	P vs. *a*	Significance Level
TOC	122,505.60	938.89	16.2	0.0006	< 0.05	High
Sw	12,168.20	811.29	9.2	0.0114	< 0.05	High
r	6,083.60	760.45	47.2	0.0209	< 0.05	High
φ	12,436.70	690.93	7.9	0.1177	> 0.05	Low
k	8,096.60	539.78	0.6	0.7982	> 0.05	Low

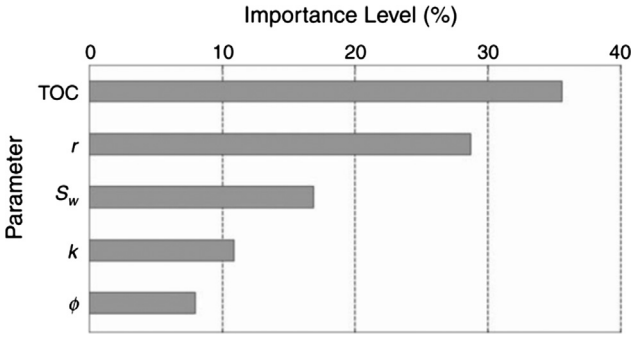

Fig. 13. Importance level of parameters affecting oil recovery [132].

almost in all the experiments, a relatively large empty space around the core are simulating hydraulic fractures and the core sample used is purely matrix. Experiments of core samples with microfracture or microcracks have not been seen in the literature yet, to the best of our knowledge. However, the existence of natural fracture network is of significant importance for the unconventional reservoir development [134]. Therefore, it should be more valuable to test the oil recovery performance using cores with natural fractures to exclude the effect of the large empty space.

To perform the huff-n-puff experiment, the first step is to measure the permeability of the core. The conventional method, or the steady-state method, might not be applicable because of many constraints. For instance, the time required to reach pressure equilibrium is very long; pressure build-up might be super high that very high-range pressure gauge is required and thus the pressure precision is compensated. The unsteady-state or the transient fluid method has been considered to advance the measurement in unconventional tight cores [135–137].

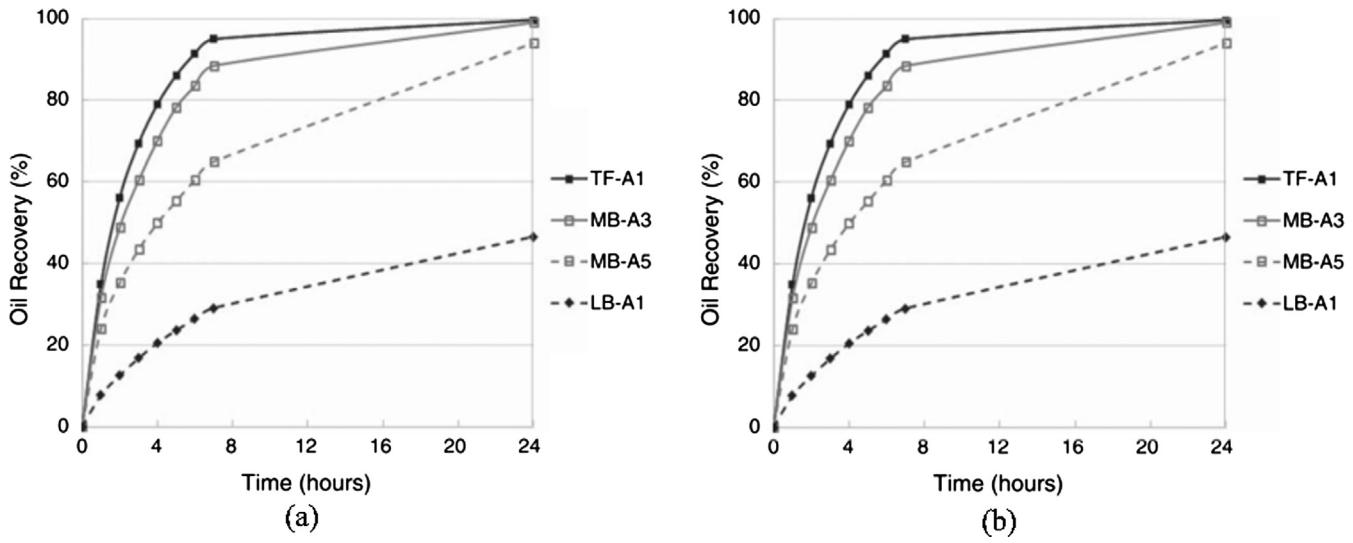

Fig. 12. Oil recovery factor as a function of time in well A (a) and Well B (b) [132].

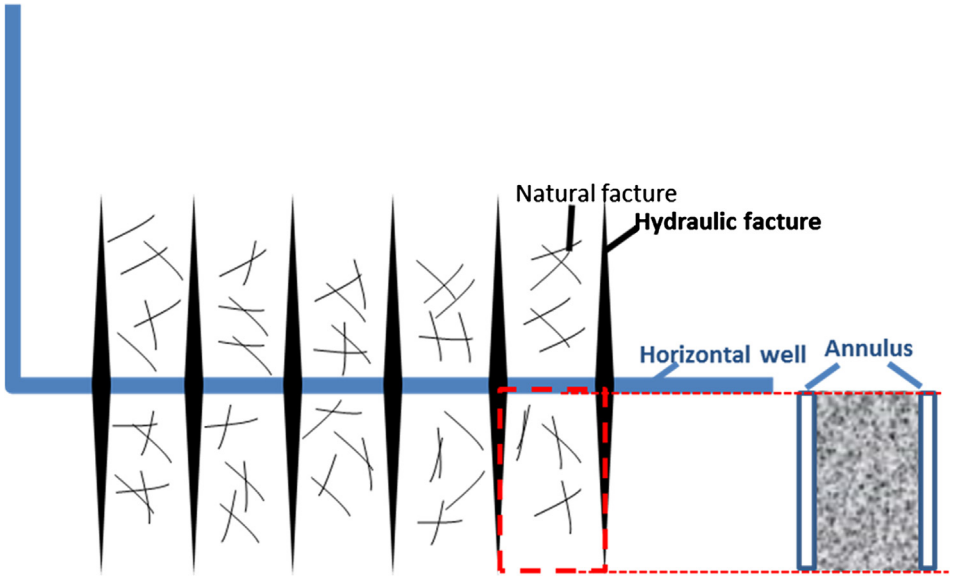

Fig. 14. Fracture and matrix system in one multi-stage hydraulic fractured well.

6.3. Approaches of measuring the permeability of shales in the laboratory

The Gas Research Institute (GRI) method was applied to measure the porosity of crushed powders. In this method, crushed powders were extracted using the Dean-Stark technique, then dried to measure porosity. Permeability was determined by the pressure-decay permeameter [138]. Several drawbacks are limiting the GRI method application for shales. First, the solvent used in the Dean-Stark extraction process dissolves kerogen in shales, causing overestimated porosity. Second, no confining pressure could be applied on the crushed powders, meaning that the in-situ stress in the deep reservoir cannot be mimicked. Third, the crushing process damaged the complex pore network in the original core sample, especially when the core sample is embedded with microfractures.

Fig. 15a shows the simplified schematic of the pulse-decay system to measure core permeability. The cylinder represents the core sample; the red oval indicates the upstream reservoir and the blue oval represents the downstream reservoir, respectively. Gas instead of liquid is frequently used as the flowing fluid because of its low viscosity. Initially, there is a pressure gap between the upstream and the other two parts. When the experiment starts, the valve is open to connect the system that the system pressure tends to reach equilibrium. Therefore, a pressure decline curve and a pressure build-up curve can be obtained after the experiment. The initial conditions are the core and the downstream are under pressure $p_{d,}$ and the upstream pressure is p_u. The boundary conditions are that the flux leaving the upstream equals the flux entering the first end surface of the core, and the flux leaving the second end surface equals the flux entering the downstream. Analytical solutions by Brace et al. [139], Hsieh et al. [140], Dicker and Smits 1988 [141], Ning [142], and Cui et al. [135] have been making progress toward providing more accurate permeability measurements, including the compressive storage effect and the gas adsorption effect. Alternatively, the numerical solution can also be applied to estimate the permeability by history matching the pressure curves.

When fractures are present in the core, either the natural fracture partially filling with cement or cracks induced by the hydraulic fracturing activity, the dual porosity and dual permeability phenomena might be revealed in the pressure curves, which can also be captured analytically or numerically [142,143]. Fig. 15b shows the flow scenario when a longitudinal fracture penetrates along the core. Gas in the fracture flows faster in the fracture that it arrives in the downstream earlier than that in the matrix, causing the fact that gas pressure in the downstream is higher than that in the core, leading to the countercurrent flow from the downstream to the core.

7. Comparison between CO_2 and other types of gas injection for EOR (and storage)

Fig. 16 shows the experimental set-up by Hawthorne et al. [144] to measure the MMP of gas with oil. Oil was initially filled in the lower part of the cell then gas was introduced to fill the upper part. The pressure of system was increased gradually to record the height variation in three capillaries with different diameters. Thermodynamically, MMP refers to the pressure that the interfacial tension between two phases becomes zero. At MMP, the capillary rise is zero based on the basic concept of Young-Laplace equation as below

$$P_c = \frac{2\sigma_F \cos\theta}{r_p} \tag{35}$$

Fig. 17 shows the methodology to estimate the MMP value. Capillary height is plotted as a function pressure with three capillaries. The intercept at the axis of pressure is predicted as the MMP when the height is zero. Hawthorne et al. [144] measured the capillary height for the Bakken crude oil with CO_2, CH_4 mixtures, and nitrogen under

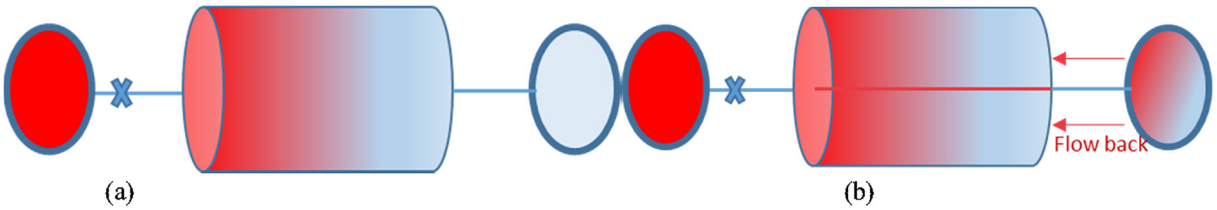

Fig. 15. Flow behaviors in the pulse-decay set-up (a) core with no fracture (b) core with fracture penetrating the longitudinal direction.

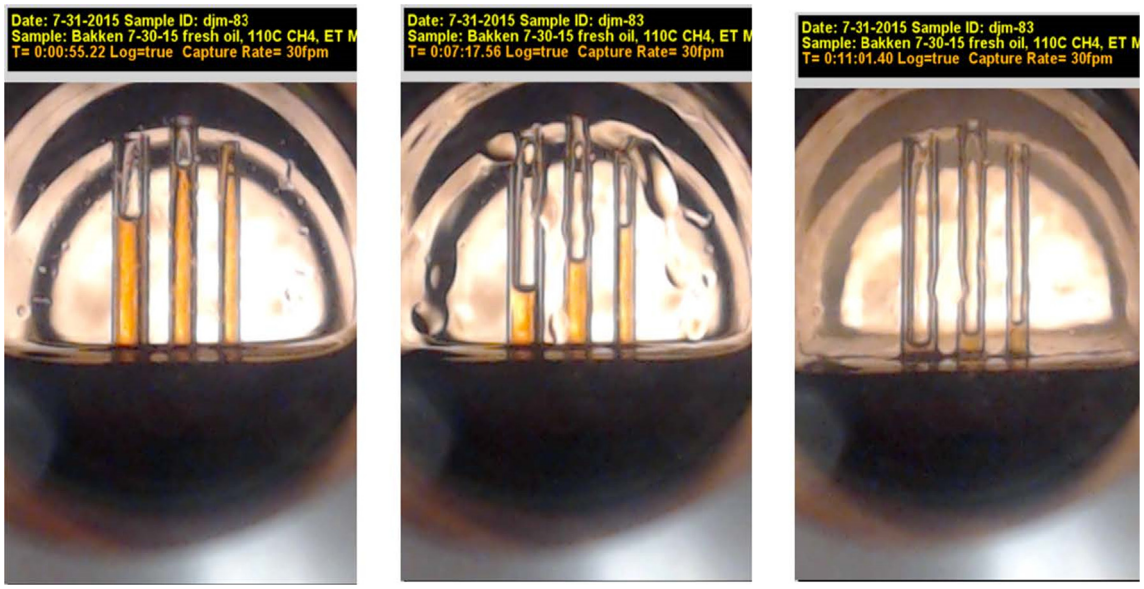

Fig. 16. The height of oil columns with various diameters under different pressures [144].

different pressures. Fig. 17 shows the laboratory results for CO_2, CH_4 mixtures under 230 °F and N_2 under 107.6 °F. The experiments were not continued until the height equaled zero because of the pressure limit of the apparatus in Fig. 17b. The CO_2 MMP with the Bakken crude oil is estimated to be 2524 psi and 1279 psi (average) under 230 °F and 107.6 °F, respectively. CH_4/CO_2 mixture MMP increases linearly and CH_4/C_2H_6 mixture MMP increases nonlinearly as a function of CH_4 percentage. The pure CH_4 MMP and C_2H_6 MMP were estimated as 4514 psi (average) and 1345 psi (average) under 230 °F, respectively. The N_2 MMP was extrapolated as 22,365 psi under 107.6 °F. As stated previously, CO_2 dissolution into the oil and oil vaporization into CO_2 are the main contributing mechanisms to recover oil in the matrix. Thus it could be predicted that the N_2 oil recovery mechanisms are significantly different from CO_2 considering the low dissolution of N_2 in oil and the extremely high MMP. The experimental work by Morel et al. [145] and the later modeling work by Hua et al. [146] well characterized the N_2 interaction with oil in the matrix/fracture system.

Previously in Fig. 3 it shows that oil swelling and vaporization are the main recovery mechanisms by CO_2 injection in the matrix/fracture system. Mechanisms of oil recovery by nitrogen is different from that of CO_2. First, the difference between different types of gas can be reviewed at the molecule level: CO_2 interacts with crude oil as molecule cluster under the supercritical state. The quadrupole-quadrupole interaction between CO_2 and oil causes oil swelling and the reduction of oil viscosity. In contrast, N_2 is more stable that its Van der Waals force with oil is very weak that the solubility in oil is very low. Oil viscosity increases in the presence of N_2 because the intermolecular distance decreases. CH_4 has strong Van der Waals force with oil making it prone to be soluble in oil. Unlike CO_2, it does not have quadrupole moment resulting in very low intermolecular force. Morel et al. [145] performed nitrogen diffusion and oil recovery experiment in the matrix/block system composing of single block matrix with one long fracture at the top. Fig. 18 shows the layout for the experiment which is similar to Fig. 3. Pure nitrogen was flowing at a constant rate in the fracture above the matrix block. Initially, methane and pentane were saturated in the matrix block under equilibrium state. Hua et al. [145] analytically and numerically modeled the diffusion and oil recovery process by successfully matching the experimental results by Morel et al. [144]. Unlike CO_2, nitrogen has higher capillary pressure with the oil phase, which is higher at the core surface and lower at the lower part of the core and as the production period goes on the capillary gradient is more obvious. The capillary pressure gradient pushes the hydrocarbons,

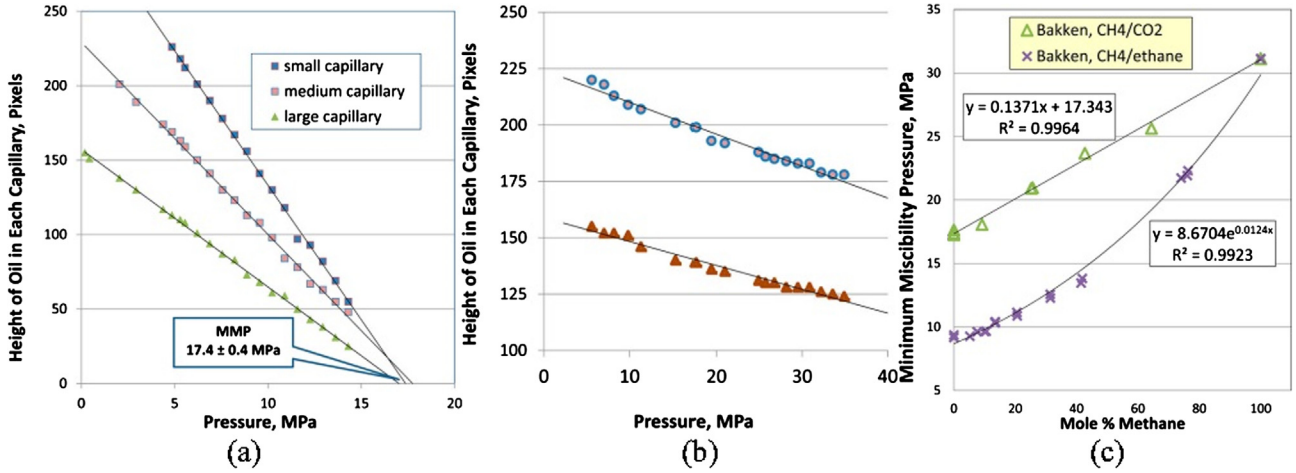

Fig 17. (a) The height of Bakken crude oil column as a function of pressure with the small capillary, medium capillary, and large capillary when the gas is CO_2 under 230 °F. (b) The height of Bakken crude oil column as a function of pressure with medium capillary, and large capillary when the gas is N_2 under 107.6 °F. (c) MMP of CH_4/CO_2 and CH_4/C_2H_6 with Bakken crude oil under 230 °F [144].

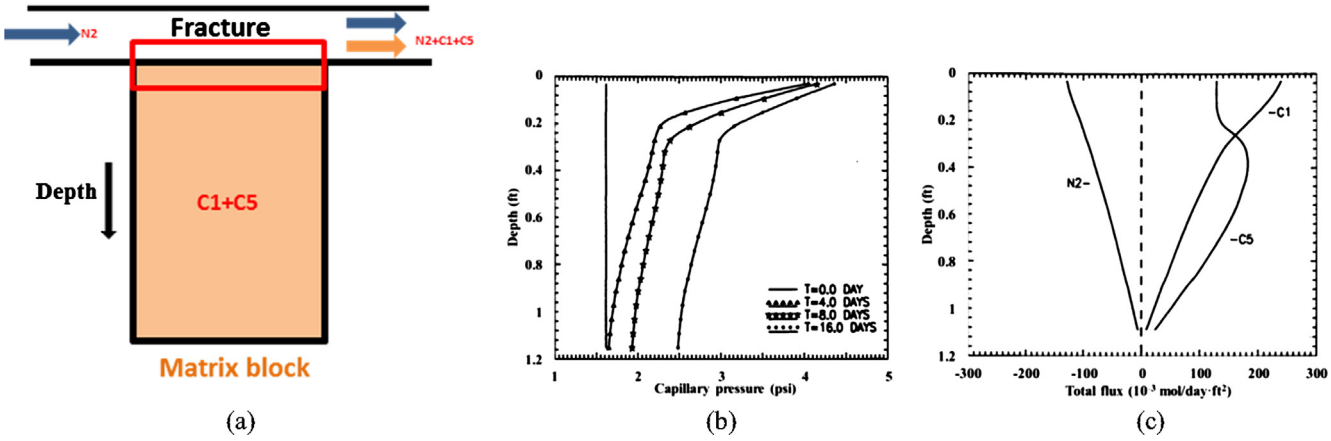

Fig. 18. (a) Schematic of nitrogen diffusion experiment; (b) capillary pressure at 0.0, 4.0, 8.0, and 18.0 days. (c) total flux of nitrogen, methane, and pentane; (Modified from Hua et al. [133]).

methane, and pentane, upward in the form of bulk or Darcy flow. The oil recovery mechanism is like "sucked out" by the capillary pressure gradient [147]. Nitrogen flows downward mainly by molecular diffusion. Therefore, gas saturation is higher at the lower part of the core, which is contrary to our intuition (Fig. 18c). The rate of molecular diffusion of nitrogen, along with the injection rate of gas in the fracture, are the two factor affecting the oil production behavior the most. Hua et al. [146] mentioned the importance of accurately taking into account of the effect of molecular diffusion and updating the capillary pressure in response to the change of interfacial tension caused by the composition change.

Ning and Kazemi [9] proposed to use ethane-enriched gas as a promising injection fluid, which contains 47.6% of methane, 12.0% of ethane, 8.0% of propane, and 1.5% of CO_2. There are several advantages of this mixture gas over pure CO_2. They discussed the difference regarding availability, infrastructure, economics, properties, operation. Ethane production is enormous producing from the volatile wells that its price is dropping at the same time, making it more cost-effective; at the same time, the infrastructure storing and transporting ethane is mature in many shale plays, like the Bakken, Eagle Ford, and Marcellus; besides, ethane is not corrosive saving the trouble of preventing corrosion in the pipelines. Also, ethane generally has lower MMP with oil than CO_2 making it more miscible with oil.

Pu et al. [148] included the adsorption effect by an algorithm of local density optimization in their core-scale gas oil recovery numerical experiment in shales along with the alternated phase behavior caused by nonporous, capillarity expressed by the J-function, and pore size distribution. Fig. 19 shows the gas storage amount during the gas injection process. Fig. 19a and b present results of N_2 and CO_2, respectively. The gas applied were flue gas composed of CO_2 and N_2. Their results show that the capillarity is one important mechanism contributing to CO_2 storage in shales and PSD is an important factor. CO_2 has the superior storage capacity to N_2 because of molecular sieving and shale adsorption selectivity.

8. Storage capacity and the associated effects on flow behavior

8.1. Gibbs/excess and absolute adsorption

First of all, it is necessary to clarify the concept of adsorption from absorption. "Adsorption" refers to the process occurring on the surface while "absorption" refers to the process of dissolution into the matrix [149], and the general word "sorption" includes both adsorption and absorption. Adsorption usually has two forms of expression: absolute adsorption and Gibbs or excess adsorption. The relationship between absolute and Gibbs adsorption is as follow [150–152]

$$V_A = \frac{V_G \rho_a}{\rho_a - \rho_g} \tag{36}$$

In this equation, ρ_a refers to the density of the adsorption phase, and ρ_g refers to the density of the free gas. Most frequently, in the laboratory, the adsorption measure is the Gibbs value, which is based on the

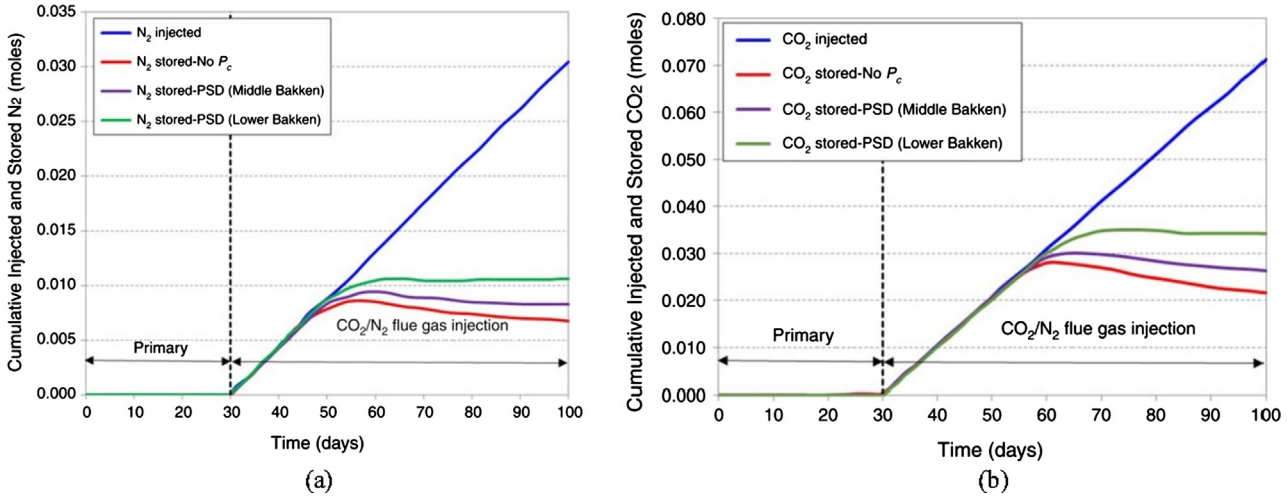

Fig. 19. Injected and stored amount of (a) N_2 and (b) CO_2 in the flue gas [148].

assumption that the sorption does not occupy volume. It could be inferred that to estimate the absolute adsorption from the value of the adsorption phase should be known. However, it is an uncertain parameter that different models might give different values [153]. In terms of calculation, the Gibbs adsorption does not consider the volume occupied by the adsorption phase in the pore space [150,151].

The Langmuir model has frequently been to characterize adsorption profile, which is based on assumptions that adsorption is a monolayer, and the adsorption phase and the free gas are under equilibrium state, and no interaction exists between adsorbed molecules [155]. Fig. 20 shows the excess adsorption profiles of CO_2 and CH_4 on three shale samples. It could be observed that there is a positive relationship between the TOC percentage and the adsorption amount, indicating that the affinity of the adsorptive gas and kerogen is the main reason of high adsorption capacity [156,157]. Methane adsorption increases linearly with pressure and the carbon dioxide adsorption increases then decreases.

8.2. Relationships between gas storage and gas flow behavior

Based on mass balance, the total gas amount equals to the free gas mass and adsorption mass.

$$\rho_g \phi_a = \phi_{void}\rho_g + \rho_a(1-\phi_{void}) \tag{37}$$

where ϕ_a is the apparent volume of total free gas after the adsorption phase changes to free gas, ϕ_{void} is the porosity consisting only of the void volume which is considered to be a constant, ρ_a is the density of adsorbate, and it is worth noting that in this mass balance equation, the profile of the Gibbs instead of the absolute adsorption should be applied because ϕ_{void} does not consider the volume of the adsorbed molecules on the pore surface. The reason is that when measuring adsorption, the Gibbs adsorption does not consider the volume occupied by the adsorption volume while the absolute adsorption does consider the adsorption volume. If the left-hand side and right-hand side are both divided by ρ_g, Eq. (37) becomes

$$\phi_a = \phi_{void} + (1-\phi_{void})\frac{\rho_a}{\rho_g} \tag{38}$$

It could be observed that the apparent porosity is only related to the ratio between ρ_a and ρ_g. Therefore, the apparent porosity of porous media as a function of pore pressure can be estimated if the adsorption profile is obtained.

The governing equation of adsorptive gas is as below

$$\frac{\partial}{\partial l}\left(\frac{\rho_g k_a \partial p}{\mu \partial l}\right) = \frac{\partial(\phi_a \rho_g)}{\partial t} \tag{39}$$

If we take the derivative of the right-hand side of Eq. (39), and substitute Eq. (38) into Eq. (39). Eq. (39) becomes

$$\frac{\partial}{\partial l}\left(\frac{\rho_g k_a \partial p}{\mu \partial l}\right) = \left[\phi_{void} + (1-\phi_{void})\frac{\partial \rho_{ad}}{\partial \rho_g}\right]\frac{\partial \rho_g}{\partial t} \tag{40}$$

The effect of adsorption on the flow behavior can be estimated by incorporating it into the flow governing equation as below [137,143]

$$\frac{\partial}{\partial l}\left(\frac{\rho_g k_a \partial p}{\mu_g \partial l}\right) = \left[\phi_{void} + (1-\phi_{void})\frac{\partial \rho_a}{\partial \rho_g}\right]\frac{\partial \rho_g}{\partial t} \tag{41}$$

where μ_g is the gas viscosity, and K_a is one variable formed during the organization of the governing equation [143], which is defined as the gradient of density of the adsorption phase over the free gas phase

$$K_a = \left(\frac{\partial \rho_a}{\partial \rho_g}\right)_T \tag{42}$$

The porosity term involved in Eq. (41) is defined as ϕ_{app}

$$\phi_{app} = \phi_{void} + (1-\phi_{void})\frac{\partial \rho_a}{\partial \rho_g} \tag{43}$$

It is observed that ϕ_{app} is the porosity that should be applied to be integrated into reservoir simulations considering the adsorptive gas, which is different from ϕ_a. More details regarding flow behavior and adsorption can consult references of [135] and [152].

9. Economics

One of the major operating and capital cost for the CO_2-related project is from CO_2 injection and storage. CO_2 can be obtained from flue gas after separation, and power plants nearby. CO_2 transportation in the pipelines and tubing underground might cause corrosion that the measures taken to prevent, like surface coating and cathodic protection, need additional capital cost [158]. Before injection into the subsurface, the gas needs to be compressed to high-pressure requiring the compressors which is another source of cost [159]. The cost of purchasing CO_2 can be compensated if the local government approves the carbon tax or the current low oil price changes [154] that co-optimization of carbon storage and enhanced oil recovery needs to be performed. The following formula shows the simplified equation of calculating the NPV [160].

$$NPV = \sum_{t=1}^{T_{cu}} \frac{C_t}{(1+r)^t} - C_0 \tag{44}$$

In this equation, T_{cu} is the cumulative time, t is the time step, C_t is the period cash inflow, r is the period discount rate, C_o is the initial investment. The total cash inflow can be expressed as

$$C = FOPT \times \$/bbl - FICIT \times \$/Ton - FWPT \times \$/dwat + FCO_2TR \times \$TAX/TON \tag{45}$$

where FOPT is the produced amount of oil, FICIT is the purchasing and injection amount of CO_2, FWPT is the amount of produced water, FCO_2STR is the amount of CO_2 stored subsurface. \$/bbl is the oil price, \$/Ton is the cost of purchasing and injecting CO_2 per ton, \$TAX/TON refers to the carbon tax.

In comparison, nitrogen, recycled lean gas or the flue gas have advantages of more sources and less expensiveness [161,162], and the natural gas injection cost can be expected to be reduced given the rapid production momentum of shale gas.

If the cyclic gas injection process is applied, decisions regarding the huff-n-puff schedule needs to be optimized for the best NPV, because during the gas injection and the soaking (well shut-in) oil production is terminated. Chen et al. [22] showed in their models that the huff-n-puff production sometimes may not reach the oil recovery by the primary

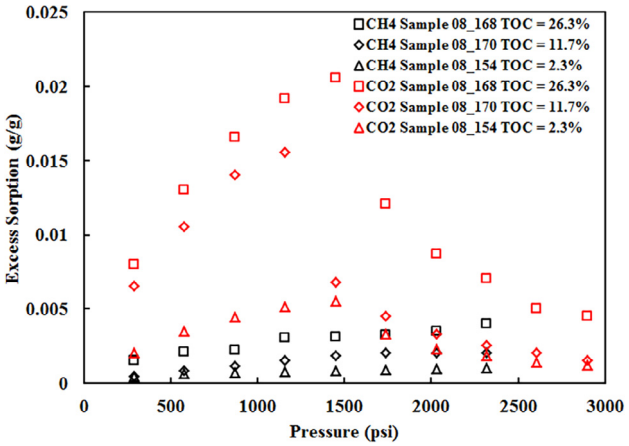

Fig. 20. Excess adsorption of CO_2 and CH_4 in shale samples (Data from Weniger et al. [154]).

production because the soak time is too long. Sheng [163] set the oil recovery factor as an objective function and set the injection, shut-in, and production time as variables and found that soaking period might not be necessary; and the optimal number of cycles need to be performed depending on the determination of an economical oil production rate. To perform a comprehensive economic analysis for the cyclic gas injection as to reduce the operation cost and maximize the NPV, more parameters should be involved, such as completion mode, well number, well spacing, fracture spacing, fracture length, proppant selection and price, etc. Besides, the optimized scenario might differ much from field to field considering the large unsimilarities of characterizations between different shale reservoirs.

10. Pilot tests

Miller and Hamilton-Smith [164] recorded the gas huff-n-puff project in one conventional reservoir lasting from 1986 to 1994. The project was performed in the Big Sinking Field located in the east of Kentucky. The field has the average porosity of 13% and average permeability of 19 mD. Two types of gas were tested: mixture gas from exhaust composing of CO_2 and nitrogen and rich gas from the casing head, each of them was tested on one well. The lessons learned from the project is that applying the two types of gas for the huff-n-puff process both yield additional oil recovery with very low increased cost which is below $2.5/bbl and that using rich gas is relatively cheaper. To achieve the same recovery effect, longer soak time was needed for the exhaust gas compared with CO_2.

10.1. Pilot tests in stimulated reservoirs

The first-generation gas injection pilot tests in shale oil reservoirs were performed in the Bakken and the Eagle Ford. EOG Resources Inc. successfully performed natural gas injection into 15 mature horizontal wells of the Eagle Ford shale in South Texas by increasing the oil recovery factor from 30% to 70% [165], and prior to that, the laboratory experiment also shows optimistic result. This is the first record of increasing the net present value applying the gas injection in tight shale reservoirs. Though not much technical details have been disclosed by the company, by analyzing the wells' production behavior, people are suggesting the gas huff-n-puff approach was applied [165]. The executive vice president (EVP) of EOG, attributed the success of the pilot tests to three reasons: (1) capital cost was much reduced for the horizontal well drilled, (2) produced gas was re-injected into the formation to reduce the amount of gas purchased and the operation cost, and (3) the EOR process extends the lifetime of the well. Up to now, in the Bakken formation, five gas injection and two water injection pilot tests have been performed. Among the total seven improved oil recovery IOR tests, four applied the huff-n-puff method and one used continuous natural gas flooding.

In the Middle Bakken formation, a joint pilot test by Continental Resources, Enerplus, and XTO Energy was performed in the Elm Coulee Field with a single-stage horizontal well [166]. Cumulative CO_2 injection volume reached 2570 tons after 45 days. The scheme of huff-n-puff was applied. The well began producing after soaking for 30 days. Initially, the well production reached a peak of 160 bbl/day then dropped rapidly to 20 bbl/day continuing for a long time. About half of the injected CO_2 was recycled finally and it is difficult to estimate the impact of CO_2 injection because of the complex operation factors. The initial production peak might be contributed to purely the pressure build-up instead of the interactions between CO_2 and oil. At the end of 2008, EOG also applied horizontal well with six fracturing stages with the scheme huff-n-puff gas injection in the Parshal Field of the Middle Bakken Formation. 30 MMscf CO_2 was injected during the huff period. The result of this pilot test indicated that the CO_2 conformance control is a main problem as very early breakthrough occurred at 11 days in one offset well but not in the other three offset wells. The reason is that the Parshal field is densely fractured where CO_2 mobility is very high. The negative results revealed the importance of reservoir characterization of natural fracture system prior to the test and sweep efficiency improvement of directing fluid movement during the test. The second test by EOG was produced water injection which showed no improved oil recovery effect. A third test was first waterflooding then mixed gas and water injection, the lessons from this test is that controlling gas mobility in fractures were still the main concern.

In a short summary for this section regarding the Bakken pilot tests performed with the horizontal wells, reservoir characterization is essentially important for the implementation of gas EOR in shale reservoirs, which can be aided by a comprehensive microseismic survey to assess the distribution of propped fracture network and the shattered rock volume, by advanced logging to characterize natural fracture and fluid properties, and by special core analysis. Obtaining ample injection and production data are important to adjust operating conditions in both the test and offset wells. Fracture system leads to the high injectivity of gas and provides the main flow path for fluids moving from matrix to wellbore through hydraulic fractures; on the other hand, the high mobility of fluids in the fracture should be controlled as to improve the conformance control. Last but not least, the development of horizontal wells and the design of completion method should be compatible with the gas injection to improve the economics and operational convenience.

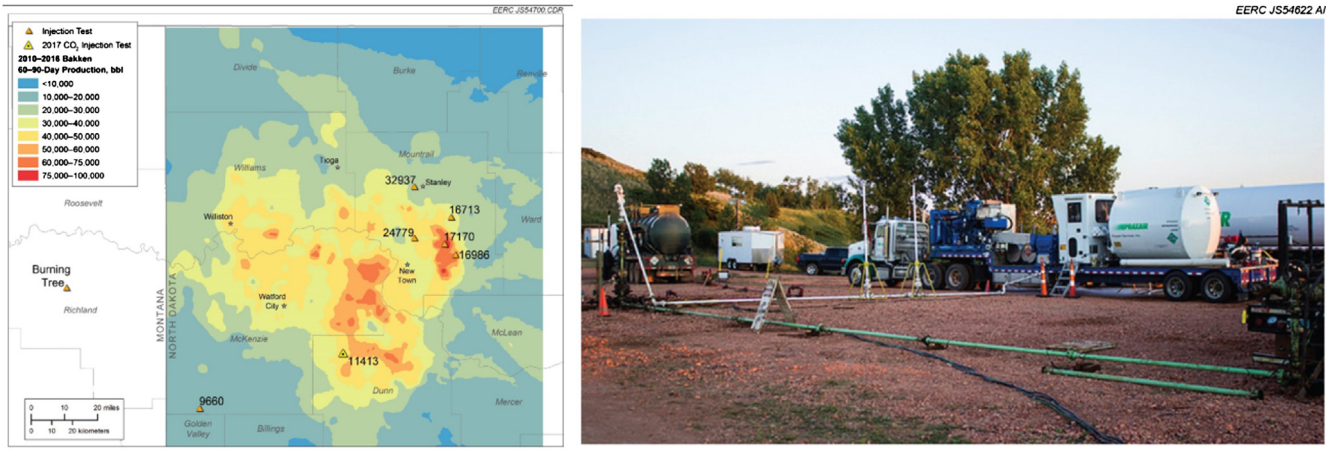

(a) (b)

Fig. 21. (a) Location of the well of the 2017 CO_2 injection test; (b) the CO2 pumping unit where the left shows the wellhead and the right shows the CO_2 truck [167].

10.2. Pilot tests in the unstimulated vertical well

In the middle of 2017, the Energy & Environmental Research Center (EERC) with the XTO Energy performed one CO_2 injection test in an unstimulated vertical well without production history [167]. The Knutson–Were well is located in the Dunn Country of North Dakota (Fig. 21). Preparatory work done before gas injection include replacing the production wellhead to injection wellhead, running pulse-neutron log (PNL) to measure petrophysical properties of the target zone, running ultrasonic imager (USI) log to check the wellbore integrity and cementing/casing status, and placing apparatus to monitor reservoir temperature and pressure changes. Two packers were placed at the top and the bottom of target zone to constrain the disperse of CO_2 plume. The CO_2 injection period is composed of two stages: the pretest test and the main test. During the pretest, totally 16 tons of CO_2 was injected less than the scheduled 60 tons because the upper packer failure occurred due to the high injection pressure. The main injection test lasted for less than 5 days composing of two cyclic injection stages, one continuous injection stage and the well shut-in stage. Totally 98.9 tons of CO_2 was injected. During the well shut-in period, the log-log pressure analysis was applied to interpret the flow behavior. Based on the classical flow regimes classifications, the flow period consists of four stages: linear flow in the fracture, bilinear flow when fracture is still open, linear flow when fracture is closed, and the pseudo-radial flow when the fracture is closed. It is observed that the linear flow with closed fracture lasted after 170 h, indicating that radial flow pattern is difficult to be formed due to the low permeability of the matrix.

Fig. 22 shows the composition analysis of oil samples in the separator after CO_2 injection in comparison to that of the original state. The x-axis is the carbon number, and the y-axis is the cumulative percentage. The steeper the line is, the higher percentage of the light component in the oil is. It could be observed that the recovered oil by CO_2 contains a large number of light components, validating the previous laboratory findings that CO_2 is able to permeate into the low-permeability shale reservoirs and extract light oil in the matrix by molecular diffusion, even when the well is not hydraulic fractured. The most important lesson from this virgin vertical well test is that CO_2 is able to be injected into the shale reservoirs without the assistance of hydraulic fracturing with the minimum injection rate of 4.5 to 5 gallons per minute, further proving the feasibility of CO_2 injection EOR and the subsequent carbon sequestration in shale oil reservoirs.

11. Conclusions

Recent progress of gas injection in shale oil reservoirs, especially the laboratory results, have shown encouraging results. Field-scale EOR projects in shale reservoirs are promising thanks to the rapid development of the hydraulic fracturing technology in the multi-stage horizontal wells. In this work we reviewed challenges and recent advancements of gas injection in terms of injection scheme, variations of shale reservoirs from conventional reservoirs, numerical simulation with the focus on fracture treatment, oil recovery mechanisms by different types of gas, results of laboratory experiments from different institutions and the pilot tests by including the most updated documents in the open literature. Detailed conclusions and suggestions are given as below.

1. Based on simulation results continuous gas flooding is preferred when the matrix permeability is larger than 0.01 mD, while in ultra-low permeability shale reservoirs the huff-n-puff scheme, or cyclic gas injection, is preferred to overcome the low gas injectivity issue. Pilot tests in the shale oil reservoirs of the United States have shown that injectivity does not pose as a main issue not only for gas injection but also for water injection, even for unstimulated wells, based on the recorded operation data, possibly due to the well development of natural fracture network. The practical concern is the conformance control because gas early breakthrough has been observed leading to the early failure of the gas injection project. An integrated approach of reservoir characterization helps characterize the fracture network prior to the project implementation, which helps decide which type of gas injection is suitable for a specific reservoir.
2. Fracture stimulation of the hydraulic fracture and natural fracture in shale reservoirs has evolved over the years and remarkable progress has been made. The appearance of EDFM approach that combining the traditional dual continuum method for the natural fracture and discrete fracture network for the hydraulic fracture, and the unstructured fracture treatment have shown to be robust and effective at possibly realistic situations. From another point of view, much work need to be done to gain meaningful simulation results of the compositional modeling of the gas injection process because many "abnormal" phenomena occur in tiny pores of the organic-rich shale, which might be significantly different from conventional oil reservoirs. Phase behavior is altered due to the pore confinement which directly affects the oil recovery performance when the phase envelope is crossed. Adsorption is important not only in terms of storage capacity but also for the flow behavior and hence the oil production behavior is different. Despite of the difficulty to avoid drawing conclusions from incomplete considerations of these multiple physics, attempts of several simulation and model work during the recent years have shown notable advances. Molecular simulation is an efficient and promising approach to overcoming limitations of exploring phase behavior in nanometer scale shale reservoirs. The authors believe that with the rapid development of molecular simulation with the aid of high-performance computing, our knowledge regarding interactions between gas and oil in shales will be refreshed and deepened.
3. Oil recovery mechanisms by different types of gas are different. For gases with low MMPs with oil, like CO_2, gas dissolution into oil and oil swell and vaporization are main mechanisms of oil recovery. For gases with very high MMPs with oil, like N_2, oil is recovered like "sucked out" from the matrix to the fracture due to the large capillary pressure gradient. Selection of gas type in the field operation largely depends on the gas accessibility and economic consideration. CO_2 utilization might be constrained because of the limited sources which can be relived if the carbon tax could be supported by the government. In contrast, enriched produced gas, flue gas have larger potentials for practical application because of the bountiful resources.

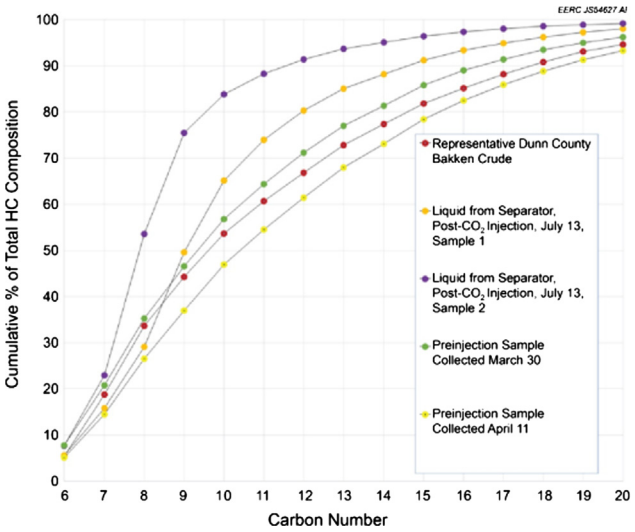

Fig. 22. Fluid composition analysis for samples before and after CO_2 injection [167].

4. Molecular diffusion is a very important flow mechanism for shale oil reservoirs with low-matrix permeability and densely fracture network. Investigations of diffusion coefficients between gas and oil under high pressure considering the low-permeability porous media effect remain scarce, and the validity of empirical correlations widely used in the oil and gas industry developed several decades ago might be questionable. A brief review of methods of measuring diffusion coefficient in the liquid-saturated pours media is provided in this work. In the future, obtaining in-situ molecular diffusion coefficient taking into account of the effect of tight porous media should be emphasized to improve the understanding of this phenomenon, so as to more accurately model diffusion during the composition and pressure changes in the matrix/fracture system that the gas injection and oil production occur.
5. Laboratory work on the core-scale experiments have shown the great potential of gas injection to rejuvenate the shale oil reservoirs after the rapid primary production. However, it is seen that most experiments use a large empty space in the core cell to mimic the hydraulic fractures, and core samples used are purely matrix without presence of natural fractures. The large volume ratio between the large empty space and volume might be the reason of the over-optimistic laboratory results. Therefore experiments of core samples with only presence of natural fractures might be of more practical significance to evaluate oil production potential from shales. In both laboratory experiments and field operations, there is a question regarding the effect of soaking period. Indeed the soaking period has been observed to improve oil recovery performance because of enhanced mixing extent between oil and gas, but it is a problem that whether or not the incremental oil recovery compensates for the loss of oil production as the system is shut in. It is more questionable in the real field operations that many operation variables should be considered as to improve the NPV.

Acknowledgments

We are grateful for the helpful discussions with Dr. Lu Jin from EERC during the course of this work. We also would like to express our gratitude to the reviewers for the recommendations to improve the quality of this work.

References

[1] EIA. 2017. Annual energy outlook 2017 with projections to 2050 2017.
[2] Jin H, Lewan D, Sonnenberg SA. Oil-generation kinetics for oil-prone Bakken shales and its implication. In: Presented at the Unconventional Resources Technology Conference (URTEC). Austin, TX, USA, Jul.24–26. 2017.
[3] Flannery J, Kraus J. Integrated Analysis of the Bakken Petroleum System. American Association of Petroleum Geologists Search and Discovery 2006; article no. 10105.
[4] Hamling Z. 2017. Developments in CO2, ethane, and rich gas EOR: a Williston basin perspective. CO2 & ROZ Conference Carbon Management Workshop. Midland, TX, USA, < http://www.co2conference.net/wp-content/uploads/2017/12/5-JHam_Midland_Dec_2017_V007_FINAL.pdf/ > ; Dec. 4; 2017 [accessed 17.04.27].
[5] Ahmed U, Meehan DN. Unconventional oil and gas resources: exploitation and development. Taylor & Francis; 2016.
[6] Dembicki H. Three common source rock evaluation errors made by geologists during prospect or play appraisals. Aapg Bull 2009;93:341–56.
[7] Sonnenberg SA, Pramudito A. Petroleum geology of the giant Elm Coulee Field, Williston Basin. Aapg Bull 2009;93:1127–53.
[8] Gong X. Assessment of Eagle Ford shale oil and gas resources [Ph.D. dissertation]. Texas A&M University; 2013.
[9] Ning Y, Kazemi H. Ethane-enriched gas injection EOR in Niobrara and Codell: a dual-porosity compositional model. SPE-190226. In: Presented at the SPE Improved Oil Recovery Conference. Tulsa, OK, USA, April.14–18. 2018.
[10] Zhang T, Baumgardner R, Ellis GS, Yang R, Travers P, Sun X, Enriquez, D. Organic matter Type, thermal maturity and gas geochemistry in Wolfcamp formation. Midland basin, TX, USA. Mar. 22. 2017.
[11] EIA. Review of emerging resources: U.S. shale gas and shale oil plays. 2011.
[12] Stevens SH, Moodhe KD, Kuuskraa VA. China shale gas and shale oil resource evaluation and technical challenges. SPE-169575. In: Presented at the SPE Asia Pacific Oil and Gas Conference and Exhibition, Jakarta, Indonesia, Oct.22–24; 2013.
[13] EIA/ARI. EIA/ARI world shale gas and shale oil resource assessment 2013.
[14] Yan J. A review of developments in carbon dioxide storage. Appl Energy 2015;148:A1–6.
[15] Patterson R. Bakken decline rates worrying for drillers, <https://oilprice.com/Energy/Crude-Oil/Bakken-Decline-Rates-Worrying-For-Drillers.html/> [accessed 17.04.27].
[16] Jia B, Tsau J, Barati R. Role of molecular diffusion in heterogeneous, naturally fractured shale reservoirs during CO_2 huff-n-puff. J Pet Sci Eng 2018;164:31–42.
[17] Chen K. Evaluation of EOR potential by gas and water flooding in shale oil reservoirs Master thesis Texas Tech University; 2013.
[18] Wan T. Evaluation of the EOR potential in shale oil reservoirs by cyclic gas injection Master Thesis Texas Tech University; 2013.
[19] Kurtoglu B. Integrated reservoir characterization and modeling in support of enhanced oil recovery for Bakken integrated reservoir characterization and modeling [Ph.D. dissertation]. Colorado School of Mines; 2014.
[20] Pu W. EOS modeling and reservoir simulation study of Bakken gas injection improved oil recovery in the Elm Coulee field, Montana Master thesis Colorado School of Mines; 2013.
[21] Fai-Yengo V, Rahnema H, Alfi M. Impact of light component stripping during CO2 Injection in Bakken formation. URTEC-1922932. In: Presented at the Unconventional Resources Technology Conference (URTEC). Denver, CO, USA, Aug.25–27. 2014.
[22] Chen C, Balhoff MT, Mohanty KK. Effect of reservoir heterogeneity on primary recovery and CO_2 Huff 'n' Puff recovery in shale-oil reservoirs. SPE Reserv Eval Eng 2014;17:404–13.
[23] Sanchez RD. Reservoir simulation and optimization of CO_2 huff-and-puff operations in the Bakken shale [MS Thesis]. University of Texas at Austin; 2014.
[24] Yu W, Lashgari HR, Sepehrnoori K. Simulation study of CO2 huff-n-puff process in Bakken tight oil reservoirs. SPE- 169575. In: Presented at the SPE Western North American and Rocky Mountain Joint Meeting. Denver, CO, USA, Apr.17–18. 2014.
[25] Yu W, Lashgari HR, Wu K, Sepehrnoori K. CO_2 injection for enhanced oil recovery in Bakken tight oil reservoirs. Fuel 2015;159:354–63.
[26] Sun J, Zou A, Sotelo E, Schechter D. Numerical simulation of CO_2 huff-n-puff in complex fracture networks of unconventional liquid reservoirs. J Nat Gas Sci Eng 2016;31:481–92.
[27] Xiong Y. Development of a compositional model fully coupled with geomechanics and its application to tight oil reservoir simulation [Ph.D. dissertation]. Colorado School of Mines; 2015.
[28] Alharthy N, Teklu TW, Kazemi H, Graves RM, Hawthorne SB, Braunberger J, et al. Enhanced oil recovery in liquid-rich shale reservoirs: laboratory to field. SPE Reserv Eval Eng 2018;21:137–59.
[29] Li L, Sheng JJ, Xu J. Gas selection for huff-n-Puff EOR in shale oil reservoirs based upon experimental and numerical study. SPE- 185066. In: Presented at the SPE Unconventional Resources Conference. Calgary, Alberta, Canada, Feb.15–16. 2017.
[30] Zuloaga-Molero P, Yu W, Xu Y, Sepehrnoori K, Li B. Simulation study of CO_2-EOR in tight oil reservoirs with complex fracture geometries. Sci Rep 2016;6:33445.
[31] Zhang Y, Di Y, Yu W, Li Z. A comprehensive model for investigation of CO2-EOR with nanopore confinement in the Bakken tight oil reservoir. In: Presented at the SPE Annual Technical Conference and Exhibition, San Antonio, Texas, USA.
[32] Yu W, Zhang Y, Varavei A, Sepehrnoori K, Zhang T, Wu K. Compositional simulation of CO2 fuff-n-puff in Eagle Ford tight oil reservoirs with CO2 molecular diffusion, nanopore confinement and complex natural fractures. In: Presented at the SPE Improved Oil Recovery Conference. Tulsa, Oklahoma, USA, Apr. 14–18. 2018.
[33] Settari A, Walter DA. Advances in coupled geomechanical and reservoir modeling with applications to reservoir compaction. SPE J 2001;3:334–42.
[34] Jaffré J, Martin V, Roberts JE. Modeling fractures and barriers as interfaces for flow in porous media. J Sci Comput 2005;26:1667–91.
[35] Talenghani AD, Olson JE. How natural fractures could affect hydraulic-fracture geometry. SPE J 2013;19:161–71.
[36] Harmelen AV, Weijermars R. Complex analytical solutions for flow in hydraulically fractured hydrocarbon reservoirs with and without natural fractures. Appl Math Model 2018;56:137–57.
[37] Barree RD, Barree VL, Craig D. Holistic fracture diagnostics: consistent interpretation of prefrac injection tests using multiple analysis methods. SPE Prod Oper 2009;24:396–406.
[38] Barree RD, Miskimins JL, Gilbert J. Diagnostic fracture injection tests: common mistakes, misfires, and misdiagnoses. SPE Prod Oper 2015;30:84–98.
[39] May JA, Anderson DS. Mudrock reservoirs—why depositional fabric and sequence stratigraphic Framework matter. AAPG Distinguished Lecture, 2012–2013 Lecture Series; 2013.
[40] Maxwell SC, Urbancic TI, Steinsberger N, Zinno R. Microseismic imaging of hydraulic fracture complexity in the Barnett shale. In: Presented at the SPE Annual Technical Conference and Exhibition. San Antonio, Texas, USA, Sep. 29-Oct. 2. 2002.
[41] Tafti TB, Aminzadeh F. Characterizing fracture network in shale reservoir using microseismic data. In: Presented at the SPE Western Regional Meeting. Bakersfield, California, USA, Mar. 21–23. 2012.
[42] Xie J, Yang C, Gupta N, King MJ, Datta-Gupta A. Integration of shale-gas-production data and microseismic for fracture and reservoir properties with the fast marching method. SPE J 2015;20:347–59.
[43] Mullen M, Pitcher J, Hinz D, Everts ML, Dunbar D, Carlstrom GM, Brenize GR. Does the presence of natural fractures have an impact on production? A case study from the Middle Bakken dolomite, North Dakota. In: Presented at the Annual Technical Conference and Exhibition. Florence, Italy, Sep. 19-22. 2010.

[44] Theloy C, Sonnenberg SA, Jin H. Integration of geological and technological aspects and their influence on production in the Bakken play, Williston Basin. 2013.
[45] Wan T, Liu H. Exploitation of fractured shale oil resources by cyclic CO_2 injection. Petrol Sci 2018.
[46] Warren JE, Root PJ. The behavior of naturally fractured reservoirs. SPE J 1963;3:245–55.
[47] Kazemi H, Merrill LS, Porterfield KL, Zeman PR. Numerical simulation of water-oil flow in naturally fractured reservoirs. SPE J 1976;16:317–26.
[48] Thomas LK, Dixon TN, Pierson RG. Fractured reservoir simulation. SPE J 1983;23:42–54.
[49] Wu Y, Pruess K. A multiple-porosity method for simulation of naturally fractured petroleum reservoirs. SPE J 1988;3:327–36.
[50] Bosma S, Hajibeygi H, Tene M, Tchelepi HA. Multiscale finite volume method for discrete fracture modeling on unstructured grids (MS-DFM). J Comput Phy 2017;351:145–64.
[51] Liang B, Jiang H, Li J, Gong C. A systematic study of fracture parameters effect on fracture network permeability based on discrete-fracture model employing finite element analyses. J Nat Gas Sci Eng 2016;28:711–22.
[52] Mayerhofer MJ, Lolon E, Warpinski NR, Cipolla CL, Walser DW, Rightmire CM. What is stimulated reservoir volume? Spe Prod Oper 2010;25:89–98.
[53] Mohaghegh SD. Reservoir modeling of shale formations. J Nat Gas Sci Eng 2013;12:22–33.
[54] Wang W, Zheng D, Sheng G, Zhang Q, Su Y. A review of stimulated reservoir volume characterization for multiple fractured horizontal well in unconventional reservoirs. Adv Geo-energy Res 2017;1:54–63.
[55] Sharma MM, Manchanda R. The role of induced un-propped (IU) fractures in unconventional oil and gas wells. In: Presented at the SPE Annual Technical Conference and Exhibition. Houston, Texas, USA, Sep. 28–30. 2015.
[56] Taleghani AD, Gonzalez M, Shojaei A. Overview of numerical models for interactions between hydraulic fractures and natural fractures: challenges and limitations. Comput Geotech 2016;71:361–8.
[57] Moinfar A, Narr W, Hui M, Mallison BT, Lee SH. Comparison of discrete-fracture and dual-permeability models for multiphase flow in naturally fractured Reservoirs. In: Presented at the SPE Reservoir Simulation Symposium. The Woodlands, Texas, USA, Feb. 21–23. 2011.
[58] Xu Y, Filho C, Yu W, Sepehrnoori K. Discrete-fracture modeling of complex hydraulic-fracture ceometries in reservoir simulators. SPE Reserv Eng 2017;20:403–22.
[59] Green DW, Willhite GP. Enhanced oil recovery. SPE Textbook Series vol. 6. 1988.
[60] Chen B, Reynolds AC. Ensemble-based optimization of the water-alternating-gas-injection process. SPE J 2016:786–98.
[61] Chen B, Reynolds AC. Optimal control of ICV's and well operating conditions for the water-alternating-gas injection process. J Petrol Eng Sci 2017;149:623–40.
[62] Hawthorne SB, Gorecki CD, Sorensen JA, Steadman EN, Harju JA, Melzer S. Hydrocarbon Mobilization Mechanisms from Upper, Middle, and Lower Bakken Reservoir Rocks Exposed to CO2. In: Presented at the SPE Unconventional Resources Conference. Calgary, Alberta, Canada. Nov. 5–7. 2013.
[63] Willhite GP, Byrnes AP, Dubois MK, Pancake RE, Tsau J, Daniels JR, et al. A pilot carbon dioxide test, Hall-Gurney Field Kansas. SPE Reserv Eval Eng 2012;15:520–32.
[64] Han J, Lee M, Lee W, Lee Y, Sung W. Effect of gravity segregation on CO_2 sequestration and oil production during CO_2 flooding. Appl Energy 2016;161:85–91.
[65] Singh H. Impact of four different CO_2 injection schemes on extent of reservoir pressure and saturation. Adv Geo-energy Res 2018;2:305–18.
[66] Yoosook H, Maneeintr K, Boonpramote T. CO_2 utilization for enhance oil recovery with huff-n-puff process in depleting heterogeneous reservoir. Energy Proc 2017;141:184–8.
[67] Zuloaga P, Yu W, Miao J, Sepehrnoori K. Performance evaluation of CO_2 huff-n-puff and continuous CO_2 injection in tight oil reservoirs. Energy 2017;134:181–92.
[68] Hoffman BT, Evans JG. Improved oil recovery IOR pilot projects in the Bakken formation. SPE-180270. In: Presented at the SPE Low Perm Symposium. Denver, Colorado, USA, May. 5–6. 2016.
[69] Christensen JR, Stenby EH, Skauge A. Review of WAG field experience. In: International Petroleum Conference and Exhibition of Mexico. Villahermosa, Mexico, Mar. 3–5. 1998.
[70] Chen B, Reynolds AC. CO_2 Water-alternating-gas injection for enhanced oil recovery: optimal well controls and half-cycle lengths. Comput Chem Eng 2018;113:44–56.
[71] Chen B. A stochastic simplex approximate gradient for production optimization of WAG and continuous water flooding [Ph.D. dissertation]. The University of Tulsa; 2017.
[72] Tsau J. Near miscible carbon dioxide application in Arbuckle reservoirs to improve oil recovery. TORP IOR Conference. Wichita, Kansas, USA, <https://torp.drupal.ku.edu/sites/torp.drupal.ku.edu/files/docs/rpsea2/RPSEA_TORP2011_near_miscible1.pdf>; Apr. 6–7; 2011 [accessed 17.04.27].
[73] Alavian SA. Modeling CO_2 injection in fractured reservoirs using single matrix block systems [Ph.D. dissertation]. Norwegian University of Science and Technology; 2011.
[74] Shafikova GM. Analysis of diffusion models in Eclipse 300 Master thesis Norwegian University of Science and Technology; 2013.
[75] Perkins TK, Johnston OC. A review of diffusion and dispersion in porous media. SPE J 1963;3:70–84.
[76] Archie GE. The electrical resistivity log as an aid in determining some reservoir characteristics. Petrol Trans AIME 1942;146:54–62.
[77] Archie GE. Introduction to petrophysics of reservoir rocks. Am Assoc Pet Geol B 1950;34:943–61.
[78] Shen L, Chen Z. Critical review of the impact of tortuosity on diffusion. Chem Eng Sci 2007;62:3748–55.
[79] Ghasemi M, Astutik W, Alavian SA, Whitson CH, Sigalas L, Olsen D, Suicmez VS. Determining diffusion coefficients for carbon dioxide injection in oil-saturated chalk by use of a constant-volume-diffusion method. SPE J 2017;22:505–20.
[80] Fernø MA, Hauge LP, Rognmo AU, Gauteplass J, Graue A. Flow visualization of CO2 in tight shale formations at reservoir conditions. Geophys Res Lett 2015;42:7414–9.
[81] Hoteit H, Firoozabadi A. Numerical modeling of diffusion in fractured media for gas injection and recycling schemes. In: Presented at the SPE Annual Technical Conference and Exhibition. San Antonio, Texas, USA. Sep. 24–27. 2006.
[82] Hoteit H. Proper modeling of diffusion in fractured reservoirs. In: Presented at the SPE Reservoir Simulation Symposium. The Woodlands, Texas, USA. Feb. 21–23. 2011.
[83] Wilke CR, Chang P. Correlation of diffusion coefficients in dilute solutions. AICHE J 1955;1:264–70.
[84] Reid RC, Prausnitz JM, Poling BE. The properties of gases & liquids. McGraw-Hill Inc; 1987.
[85] Sigmund PM. Prediction of molecular diffusion at reservoir conditions. Part II-estimating the effects of molecular diffusion and convective mixing in multicomponent systems. J Can Petrol Technol 1976;15:53–62.
[86] Whitson CH, Brule MR. Phase behavior. Society of Petroleum Engineers; 2000.
[87] da Silva FV, Belery P. Molecular diffusion in naturally fractured reservoirs: a decisive recovery mechanism. In: Presented at the SPE Annual Technical Conference and Exhibition. San Antonio, Texas. USA. Oct. 8–11. 1989.
[88] Sigmund PM. Prediction of molecular diffusion at reservoir conditions. Part 1-measurement and prediction of binary dense gas diffusion coefficients. J Can Petrol Technol 1976;15:48–57.
[89] Renner TA. Measurement and correlation of diffusion coefficients for CO_2 and rich-gas applications. SPE Reserv Eng 1988;3:517–23.
[90] Li Z, Dong M. Experimental study of carbon dioxide diffusion in oil-saturated porous media under reservoir conditions. Ind Eng Chem Res 2009;48:9307–17.
[91] Ménard R. A comparison of correlation-length estimation methods for the objective analysis of surface pollutants at environment and climate change Canada. J Air Waste Manag 2016;66:874–95.
[92] Jensen JL, Currie ID. A new method for estimating the Dykstra-Parsons coefficient to characterize reservoir heterogeneity. SPE Reserv Eng 1990;5:369–74.
[93] Maschio C, Schiozer DJ. A new upscaling technique based on Dykstra-Parsons coefficient: evaluation with streamline reservoir simulation. J Petrol Sci Eng 2003;40:27–36.
[94] Ren B, Sun Y, Bryant S. Maximizing local capillary trapping during CO_2 injection. Energy Procedia 2014;63:5562–76.
[95] Garmeth G, Johns RT. Upscaling of miscible floods in heterogeneous reservoirs considering reservoir mixing. SPE Reserv Eval Eng 2010;13:747–63.
[96] Li L, Sheng JJ. Upscale methodology for gas huff-n-puff process in shale oil reservoirs. J Pet Sci Eng 2017;153:36–46.
[97] Bahadori A. Fluid phase behavior for conventional and unconventional oil and gas reservoirs. Gulf Professional Publishing; 2017.
[98] Jin B, Bi R, Nasrabadi H. Molecular simulation of the pore size distribution effect on phase behavior of methane confined in nanopores. Fuel 2017;452:94–102.
[99] Yang G, Fan Z, Li X. Determination of confined fluid phase behavior using modified Peng-Robinson equation of state. In: Presented at the Unconventional Resources Technology Conference. Houston, TX, USA, Jul.23–25. 2018.
[100] Lowry E, Piri M. Effects of chemical and physical heterogeneity on confined phase behavior in nanopores. Microporous Mesoporous Mater 2018;263:53–61.
[101] Zarragoicoechea GJ, Kuz VA. Critical shift of a confined fluid in a nanopore. Fluid Phase Equilib 2004;220:7–9.
[102] Singh SK, Sinhtoragea A, Deo G, Singh K. Vapor – liquid phase coexistence, critical properties, and surface tension of confined alkanes. J Phys Chem C 2009;113:7170–80.
[103] Devegowda D, Sapmanee K, Civan F, Sigal RF. Phase behavior of gas condensates in shales due to pore proximity effects: implications for transport, reserves and well productivity. In: Presented at the SPE Annual Technical Conference and Exhibition. San Antonio, Texas, USA. Oct. 8–10. 2012.
[104] Ma Y, Jin L, Jamili A. Modifying van der Waals equation of state to consider Influence of confinement on phase behavior. In: Presented at the SPE Annual Technical Conference and Exhibition. New Orleans, Louisiana, USA, Sep 30–Oct 2. 2013.
[105] Jin L, Ma Y, Jamili A. Investigating the effect of pore proximity on phase behavior and fluid properties in shale formations. In: Presented at the SPE Annual Technical Conference and Exhibition. New Orleans, Louisiana, USA, Sep 30–Oct 2. 2013.
[106] Li L, Sheng JJ. Nanopore confinement effects on phase behavior and capillary pressure in a Wolfcamp shale reservoir. J Taiwan Inst Chem 2017;78:317–28.
[107] Nojabaei B, Johns RT, Chu L. Effect of capillary pressure on phase behavior in tight rocks and shales. SPE Reserv Eval Eng 2013;16:281–9.
[108] Pedersen KS, Christensen PL. Phase behavior of petroleum reservoir fluids. Taylor & Francis Group; 2007.
[109] Haider BA. Impact of capillary pressure and critical properties shift due to confinement on hydrocarbon production from shale reservoirs [Ph.D. dissertation]. Stanford University; 2015.
[110] Wang Y, Yan B, Killough J. Compositional modeling of tight oil using dynamic nanopore properties. In: Presented at the SPE Annual Technical Conference and Exhibition. New Orleans, Louisiana, USA, Sep. 3–Oct. 2. 2013.
[111] Jin Z, Firoozabadi A. Thermodynamic modeling of phase behavior in shale media. SPE J 2016;21:190–207.
[112] Huang L, Tang M, Fan M, Cheng H. Density functional theory study on the reaction

between hematite and methane during chemical looping process. Appl Energy 2015;159:132–44.
[113] Baležentis T, Streimikiene D. Multi-criteria ranking of energy generation scenarios with Monte Carlo simulation. Appl Energy 2017;185:862–71.
[114] Aljamaan H, Ismail MA, Kovscek AR. Experimental investigation and Grand Canonical Monte Carlo simulation of gas shale adsorption from the macro to the nano scale. J Nat Gas Sci Eng 2017;48:119–37.
[115] Wang S, Javadpour F, Feng Q. Molecular dynamics simulations of oil transport through inorganic nanopores in shale. Fuel 2016;171:74–86.
[116] Wang S, Javadpour F, Feng Q. Fast mass transport of oil and supercritical carbon dioxide through organic nanopores in shale. Fuel 2016;181:741–58.
[117] Heller R, Vermylen J, Zoback MD. Experimental investigation of matrix permeability of gas shales. AAPG Bull 2014;98:975–95.
[118] Jin B, Li D, Tsau J, Barati R. Gas permeability evolution during production in the Marcellus and Eagle Ford shales: coupling diffusion/slip-flow, geomechanics, and adsorption/desorption. In: Presented at the SPE Unconventional Resources Technology Conference. Austin, Texas, USA, July 24–26. 2017.
[119] Jia B, Tsau J, Barati R. A workflow to estimate shale gas permeability variations during the production process. Fuel 2018;220:879–89.
[120] Zhang Y, Yu W, Li Z. Simulation study of factors affecting CO_2 huff-n-puff process in tight oil reservoirs. J Pet Sci Eng 2018;163:264–9.
[121] Das SK, Butler RM. Diffusion coefficients of propane and butane in peace river bitumen. J Can Chem Eng 1996;74:985–92.
[122] Wang LS, Lang ZX, Guo TM. Measurements and correlation of the diffusion coefficients of carbon dioxide in liquid hydrocarbons under elevated pressure. Fluid Phase Equilib 1996;117:364–72.
[123] Riazi MR. A new method for experimental measurement of diffusion coefficients in reservoir fluids. J Pet Sci Eng 1996;14:235–50.
[124] Zhang YP, Hyndman CL, Maini BB. Measurement of gas diffusivity in heavy oils. J Pet Sci Eng 2000;25:37–47.
[125] Guo P, Wang Z, Shen P, Du J. Molecular diffusion coefficients of the multicomponent gas-crude oil systems under high temperature and pressure. Ind Eng Chem Res 2009;48:9023–7.
[126] Eide O, Ferno MA, Graue A. Visualization of CO2 EOR by diffusion in fractured chalk. In: Presented at the SPE Annual Technical Conference and Exhibition. Amsterdam, The Netherlands, Oct. 27-29. 2014.
[127] CMG. Gem user guide compositional & unconventional reservoir Simulation 2016.
[128] Teng Y, Liu Y, Song Y, Jiang L, Zhao Y, Zhou X, Zheng H, Chen J. A study on CO2 diffusion coefficient in n-decane saturated porous media by MRI. In: Presented at the 6th International Conference on Applied Energy-ICAE 2014.
[129] Afsahi S, Kantzas A. Advances in diffusivity measurement of solvents in oil sands. In: Presented at Canadian International Petroleum Conference. Calgary, Alberta, Canada, June 13–15. 2006.
[130] Tovar FD, Eide O, Graue, Arne et al. 2014. Experimental investigation of enhanced recovery in unconventional liquid reservoirs using CO2: a look ahead to the future of unconventional EOR. In: Presented at the SPE Unconventional Resources Conference. The Woodlands, Texas, USA. Apr. 1–3. 2014.
[131] Song C, Yang D. Experimental and numerical evaluation of CO_2 huff-n-puff processes in Bakken formation. Fuel 2017;190:145–62.
[132] Jin L, Sorensen JA, Hawthorne SB, Smith SA, Pekot LJ, Bosshart NW, et al. Improving oil recovery by use of carbon dioxide in the Bakken unconventional system: a laboratory Investigation. SPE Reserv Eval Eng 2017;20:602–12.
[133] Jin L, Hawthorne S, Sorensen J, Pekot L, Kurz B, Smith S, et al. Advancing CO2 enhanced oil recovery and storage in unconventional oil play—experimental studies on Bakken shales. Appl Energy 2017;208:171–83.
[134] Wang X, Ding W, Cui L, Wang R, He J, Li A, et al. The developmental characteristics of natural fractures and their significance for reservoirs in the Cambrian Niutitang marine shale of the Sangzhi block, southern China. J Pet Sci Eng 2018;165:831–41.
[135] Cui X, Bustin AMM, Bustin RM. Measurements of gas permeability and diffusivity of tight reservoir rocks: different approaches and their applications. Geofluids 2009;9:208–23.
[136] Faruk C, Rai CS, Sondergeld CH. Determining shale permeability to gas by simultaneous analysis of various pressure tests. SPE J 2012;17:717–26.
[137] Jia B, Tsau J, Barati R. Evaluation of core heterogeneity effect on pulse-decay experiment. In: Presented at International Symposium of the Society of Core Analysts. Vienna, Austria, Aug. 27–Sep. 1. 2017.
[138] Gas Research Institute (GRI). Developing of laboratory and petrophysical techniques for evaluating shale reservoirs. Final report 1996.
[139] Brace WF, Walsh JB, Frangos WT. Permeability of granite under high pressure. J Gephys Res 1968;73:2225–36.
[140] Hsieh PA, Tracy JV, Neuzil CE, Bredehoeft JD, Silliman SE. A transient laboratory method for determining the hydraulic properties of 'tight' rocks—I Theory. Int J Rock Mech Min 1981;18:245–52.
[141] Dicker AI, Smits RM. A practical approach for determining permeability from laboratory pressure-pulse decay measurements. In: International Meeting on Petroleum Engineering. Tianjin, China. Nov. 1–4. 1988.
[142] Ning X. The measurement of matrix and fracture properties in naturally fractured low permeability cores using a pressure pulse method [Ph.D. dissertation]. Texas A &M University; 1992.
[143] Cronin MB. Core-scale heterogeneity and dual-permeability pore structure in the Barnett shale Master thesis University of Texas at Austin; 2014.
[144] Hawthorne SB, Miller DJ, Jin L, Gorecki CD. Rapid and simple capillary-rise/vanishing interfacial tension method to determine crude oil minimum miscibility pressure: pure and mixed CO_2, methane, and ethane. Energy Fuels 2016;30:6365–72.
[145] Morel D, Bourbiaux B, Latil M, Thiebot B. Diffusion effects in gasflooded light-oil fractured reservoirs. SPE Adv Tech Series 1993;1:100–9.
[146] Hua H, Whitson CH, Yuandiang Q. A study of recovery mechanisms in a nitrogen diffusion experiment. SPE-21893.
[147] Whitson CH. Gas EOR lecture notes. 2018.
[148] Pu H, Wang Y, Li Y. How CO_2-storage mechanisms are different in organic shale: characterization and simulation studies. SPE J 2017.
[149] Ertas D, Kelemen SR, Halsey TC. Petroleum expulsion part 1. Theory of kerogen swelling in multicomponent solvents. Energy Fuels 2006;20:295–300.
[150] Sudibandriyo M, Pan Z, Fitzgerald JE, et al. Adsorption of methane, nitrogen, carbon dioxide, and their binary mixtures on dry activated carbon at 318.2 K and pressures up to 13.6 MPa. Langmuir 2003;2003(19):5323–31.
[151] Sudibandriyo M, Sayeed A, Robinson RL, et al. Ono–Kondo lattice model for high-pressure adsorption: pure gases. Fluid Phase Equilib 2010;299(2):238–51.
[152] Jia B, Tsau J, Barati R. Different flow behaviors of low-pressure and high-pressure carbon dioxide in shales. SPE J 2018; Preprint.
[153] Zhou C, Hall F, Gasem KAM, Robinson RL. Predicting gas adsorption using two-dimensional equations of state. Ind Eng Chem Res 1994;33:1280–9.
[154] Weniger P, Kalkreuth W, Busch A, Kross BM. High-pressure methane and carbon dioxide sorption on coal and shale samples from the Paraná Basin, Brazil. Int J Coal Geol 2010;2010(84):190–205.
[155] Clarkson CR, Bustin RM, Levy JH. Application of the mono/multilayer and adsorption potential theories to coal methane adsorption isotherms at elevated temperature and pressure. Carbon 1997;12:1689–705.
[156] Liu K, Ostadhassan M, Zou J, Gentzis T, Rezaee R, Bubach B, Carvajal-Ortizc H. Multifractal analysis of gas adsorption isotherms for pore structure characterization of the Bakken shale. Fuel 2018;219:296–311. New Orleans, LA, USA, Oct. 4-7; 2009.
[157] Wang FP, Reed RM. Pore networks and fluid flow in gas shales. In: SPE Annual Technical Conference and Exhibition.
[158] Yevtushenko O, Bettge D, Bäßler R, Bohraus S. Corrosion of CO_2 transport and injection pipeline steels due to the condensation effects caused by SO_2 and NO_2 impurities. Mater Corrosion 2015;66:334–41.
[159] Burton M, Bryant SL. Eliminating buoyant migration of sequestered CO_2 through surface dissolution: implementation costs and technical challenges. SPE Reserv Eval Eng 2009;12:399–407.
[160] Jahangiri HR, Zhang D. Optimization of the net present value of carbon dioxide sequestration and enhanced oil recovery. In: Presented at the Offshore Technology Conference. Houston, Texas, USA. May. 2–5. 2011.
[161] Akinluyi O, Hazlett R. Enhanced-oil-recovery potential for lean-gas reinjection in zipper fractures in liquid-rich basins. SPE J 2017.
[162] Ahmadi MA, Hasanvand M, Shokrolahzadeh S. Technical and economic feasibility study of flue gas injection in an Iranian oil field. Petroleum 2015;1:217–22.
[163] Sheng JJ. Optimization of huff-n-puff gas injection in shale oil reservoirs. Petroleum 2017;3:431–7.
[164] Miller BJ, Hamilton-Smith, T. Field case: cyclic gas recovery for light oil-using carbon dioxide/nitrogen/natural gas. In: Presented at the SPE Annual Technical Conference and Exhibition. New Orleans, Louisiana, USA, Sep. 27–30. 1998.
[165] Rassenfoss S. Shale EOR works, but will it make a difference? J Petrol Technol 2017.
[166] Sorensen JA, Hamling JA. Historical Bakken test data provide critical insights on EOR in tight oil plays. Am Oil Gas Report 2016;59:55–61.
[167] Sorensen SA, Pekot LJ, Torres JA, Jin, L, Hawthorne SB, Smith SA, Jacobson LL, Doll TE. Field test of CO2 injection in a vertical middle Bakken well to evaluate the potential for enhanced oil recovery and CO2 storage. In: Presented at the Unconventional Resources Technology Conference. Houston, TX, USA, Jul. 23–25. 2018.